Charles University

Faculty of Science

Study programme: Macromolecular chemistry

Ing. Tomáš Urbánek

Supramolecular biocompatible polymer nanosystems for bioapplications

Doctoral thesis

Supervisor: prof. Mgr. Martin Hrubý, Ph.D., DSc.

Prague, 2024

Declaration

I hereby declare that I have independently worked on the submitted dissertation, and that neither this work nor any substantial part of it has been used to obtain another or the same academic degree. I also declare that I have cited all sources of information used to the best of my knowledge and belief.

Prohlášení

Prohlašuji, že předkládanou disertační práci jsem vypracoval samostatně, a že práce ani její podstatná část nebyla použita k získání jiného nebo stejného akademického titulu. Současně prohlašuji, že jsem odcitoval všechny použité informační prameny podle mého nejlepšího vědomí a svědomí.

Prague, 31st August, 2024

Ing. Tomáš Urbánek

Acknowledgments

I would like to sincerely thank my supervisor, prof. Mgr. Martin Hrubý, DSc., for his guidance, support, and mentorship.

I would like to thank the Faculty of Science at Charles University, and the Department of Physical and Macromolecular Chemistry, for giving me the opportunity to study in a supportive academic environment. I am also deeply thankful to the Institute of Macromolecular Chemistry at the Czech Academy of Sciences for offering the resources and facilities that made my research possible.

I want to thank all my colleagues at the Institute of Macromolecular Chemistry from the Department of Supramolecular Structures for their support and friendship. I am especially grateful to Jiří Trousil for his helpful collaboration, valuable discussions, and companionship.

Lastly, I want to thank my family and friends for their ongoing encouragement, patience, and support.

Table of Contents

Abstract

This thesis focuses on the development of supramolecular biocompatible polymer nanosystems for biomedical applications. Infectious diseases and inflammation pose significant challenges today, further exacerbated by the increasing prevalence of antibiotic resistance. Motivated by these urgent issues, this work aims to address these challenges comprehensively through the use of advanced polymeric systems. The thesis is organized into three main objectives, each targeting a specific aspect of this overarching problem. The first part of the thesis involves the design and characterization of block copolymers based on poly(ethylene oxide)-*b*-poly(*ε*-caprolactone), with a modification to the hydrophobic segment by introducing a second monomer, *γ*-butyrolactone. This modification aims to tailor the copolymer's biological behavior, particularly its enzymatic degradation, to optimize it for use as a drug delivery system for the antibacterial antibiotic rifampicin. The second objective explores the self-assembly behavior of chloroxine, an antimicrobial drug, focusing on the preparation of stable nanocrystalline particles via precipitation using polymeric non-ionic surfactants. This approach is intended to enhance the solubility and bioavailability of chloroxine, thereby improving its therapeutic efficacy. The third part of the thesis is dedicated to the development of a polymer-based potentiometric sensor designed for *in situ* detection of inflammation-related reactive oxygen species (ROS). The sensor features a layer composed of porphyrin cores linked by bis(thiophene) bridges, with metal ions embedded within the porphyrin structure. The entire sensor layer is shielded by covalently bonded poly(2-methyl-2-oxazoline) to prevent the adsorption of serum proteins. Upon exposure to specific ROS, the sensor exhibits a measurable change in electrical potential, with sensitivity sufficient to detect the early stages of inflammation and infection. This thesis presents a comprehensive approach to the development of polymer-based nanosystems for the treatment and detection of infectious diseases and inflammation, addressing key challenges in modern medicine.

Key words: controlled polymerization, self-assembly, nanoprecipitation, enzymatic degradation, antibacterial drug delivery, early detection of inflammation

Abstrakt

Tato práce se zaměřuje na vývoj supramolekulárních biokompatibilních polymerních nanosystémů pro biomedicínské aplikace. Infekční onemocnění a záněty představují v současné době značnou výzvu, kterou ještě zhoršuje rostoucí výskyt rezistence vůči antibiotikům. Tato práce, motivovaná těmito naléhavými problémy, si klade za cíl řešit tyto výzvy komplexně pomocí pokročilých polymerních systémů. Práce je rozdělena do tří hlavních cílů, z nichž každý se zaměřuje na specifický aspekt tohoto zastřešujícího problému. První část práce zahrnuje návrh a charakterizaci blokových kopolymerů na bázi poly(ethylenoxid)-*b*-poly(ε-kaprolakton) s modifikací hydrofobního segmentu zavedením druhého monomeru, γ-butyrolaktonu. Cílem této modifikace je upravit biologické chování kopolymeru, zejména jeho enzymatickou degradaci, a optimalizovat jej pro použití jako systém pro podávání antibakteriálního antibiotika rifampicinu. Druhý cíl zkoumá samoskladné chování chloroxinu, antimikrobiálního léčiva, se zaměřením na přípravu stabilních nanokrystalických částic srážením pomocí polymerních neiontových povrchově aktivních látek. Tento přístup má zvýšit rozpustnost a biologickou dostupnost chloroxinu, a tím zlepšit jeho terapeutickou účinnost. Třetí část práce je věnována vývoji potenciometrického senzoru na bázi polymeru určeného k detekci in situ reaktivních forem kyslíku (ROS) souvisejících se zánětem. Senzor obsahuje vrstvu složenou z porfyrinových jader spojených bis(thiofenovými) můstky, přičemž ionty kovů jsou zabudovány do porfyrinové struktury. Celá vrstva senzoru je stíněna kovalentně vázaným poly(2-methyl-2-oxazolinem), aby se zabránilo adsorpci sérových proteinů. Po vystavení specifickým ROS senzor vykazuje měřitelnou změnu elektrického potenciálu s citlivostí dostatečnou k detekci časných stadií zánětu a infekce. Tato práce představuje komplexní přístup k vývoji nanosystémů na bázi polymerů pro léčbu a detekci infekčních onemocnění a zánětu, čímž řeší klíčové problémy moderní medicíny.

Klíčová slova: řízená polymerizace, samouspořádání, nanoprecipitace, enzymatická degradace, řízené uvolňování antibakteriálních léků, raná detekce zánětu

List of symbols and abbreviations

2TTP	5,10,15,20-tetra(thien-2-yl)porphyrin
3TTP	5,10,15,20-tetra(thien-3-yl)porphyrin
ATCC	American type Culture Collection
γBL	γ-butyrolactone
BR700	Brij 700
BR92	Brij 92
εCL	ε-caprolactone
CCM	Czech collection of microorganisms
CLSM	confocal laser scanning microscopy
CMC	critical micellar concentration
CXNP	chloroxine nanoparticle
DACCA	7-(diethylamino)coumarin-3-carbonyl azide
DBU	1,8-diazabicyclo(5.4.0)undec-7-ene
DLS	dynamic light scattering
DPP	diphenyl phosphate
DSC	differential scanning calorimetry
DSM	Deutsche Sammlung von Mikroorganismen und Zellkulturen (German Collection of Microorganisms and Cell Cultures)
EIS	electrochemical impedance spectroscopy
FTO	fluorine-doped tin oxide
GC	glassy carbon
HD-PE	high-density polyethylene
LCST	lower critical solution temperature
MBC	minimum bactericidal concentration
MIC	minimum inhibitory concentration
NP	nanoparticle
PANI	polyaniline

PBS	phosphate-buffered saline
PEO	poly(ethylene oxide)
PEtOx	poly(2-ethyl-2-oxazoline)
PHA	polyhydroxyalkanoates
PHB	poly(3-hydroxybutyrate)
PHV	poly(3-hydroxyvalerate)
PHPMA	poly(*N*-(2-hydroxypropyl)methacrylamide)
PMeOx	poly(2-methyl-2-oxazoline)
PPO	poly(propylene oxide)
PVP	poly(*N*-vinyl pyrrolidone)
ROP	ring opening polymerization
ROS	reactive oxygen species
SANS	small-angle neutron scattering
SAXS	small-angle X-ray scattering
SEM	scanning electron microscopy
SLS	static light scattering
TBD	1,5,7-triazabicyclo(4.4.0)dec-5-ene
TEM	transmission electron microscopy
TEWL	transepidermal water loss
TMAH	tetramethylammonium hydroxide
TS	type strain
TU	thiourea
TW80	Tween 80
UCST	upper critical solution temperature
UHMWPE	ultra-high-molecular-weight polyethylene

List of publications and contributions at conferences

Publications included into this thesis

1) Urbánek, T.; Jägger, E.; Jägger, A.; Hrubý, M. Selectively Biodegradable Polyesters: Nature-Inspired Construction Materials for Future Biomedical Applications. *Polymers* **2019**, 11 (6), 1061. IF = 4.9
2) Urbánek, T.; Trousil, J.; Rak, D.; Gunár, K.; Konefał, R.; Šlouf, M.; Sedlák, M.; Janoušková Šebestová, O.; Hrubý, M. γ-Butyrolactone Copolymerization with the Well-Documented Polymer Drug Carrier Poly(ethylene oxide)-block-poly(ε-caprolactone) to Fine-Tune Its Biorelevant Properties. *Macromolecular Bioscience* **2020**, 20 (5). IF = 4.979
3) Trousil, J.; Matějková, J.; Dai, YS.; Urbánek, T.; Šlouf, M.; Škorič, M.; Nejedlý, T.; Hrubý, M.; Fang, JY. Nanocrystalline chloroxine possesses broad-spectrum antimicrobial activities and excellent skin tolerability in mice. *Nanomedicine (Lond)* **2022**, 17 (3), 137. IF = 5.307
4) Urbánek, T.; Ivanko, I.; Svoboda, J.; Tomšík, E.; Hrubý, M., Selective potentiometric detection of reactive oxygen species (ROS) in biologically relevant concentrations by a modified metalized polyporphyrine sensing layer coated with nonbiofouling poly(2-alkyl-2oxazoline)s. *Sensors and Actuators B: Chemical* **2022**, 363, 131827. IF = 9.221

Publications not included into this thesis

5) Trousil, J.; Syrová, Z.; Dal, NJ.; Rak, D.; Konefał, R.; Pavlova, E.; Matějková, J.; Cmarko, D.; Kubíčková, P.; Pavliš, O.; Urbánek, T.; Sedlák, M.; Fenaroli, F.; Raška, I.; Štěpánek, P.; Hrubý, M., Rifampicin Nanoformulation Enhances Treatment of Tuberculosis in Zebrafish. *Biomacromolecules* **2019**, 20 (4), 1798. IF = 6.988

Contributions at conferences

6) Urbánek, T., Trousil, J. ,Hermanová, S., Hrubý, M. Polymerization of thermodynamically unfavored monomer *γ*-butyrolactone and its medical application, Česko-slovenská konference POLYMERY 2018, Třešť, Czech Republic, 2018.
7) Urbánek, T., Trousil, J., Černoch, P., Hermanová, S., Hrubý, M. Částice poly(ε-kaprolakton-co-γ-butyrolakton)u pro medicínské použití, *69. Zjazd chemikov*, Horný Smokovec, Vysoké Tatry, Slovakia, **2017**.
8) Hrubý, M., Loukotová, L., Kučka, J., Rabyk, M., Trousil, J., Urbánek, T., Pánek, J., Lobaz, V., Kolouchová, K., Švec, P., Vetrík, M., Kománková, L., Sedláček, O., Štěpánek, P. Supramolecular polymer nanosystems for diagnostics and therapy, *Bordeaux Polymer Conference 2018*, Bordeaux, France, **2018**. (presented by Hrubý, M.)

9) Hrubý, M., Loukotová, L., Kučka, J., Rabyk, M., Trousil, J., Urbánek, T., Pánek, J., Lobaz, V., Kolouchová, K., Švec, P., Vetrík, M., Kománková, L., Sedláček, O., Štěpánek, P. Supramolekulární samouspořádané polymerní systémy pro diagnostiku a terapii, *69. Zjazd chemikov*, Horný Smokovec, Vysoké Tatry, Slovakia, **2017**. (presented by Hrubý, M.)

10) Ivanko, I., Urbánek, T., Hrubý, M., Tomšík, E. Potentiometric detection of reactive oxygen species (ROS) by metalized polyporphyrine layer coated by nonbiofouling film, *19. Matrafured – International Meeting on Chemical Sensors*, Visegrad, Hungary, **2022**. (presented by Ivanko, I.)

1. Theoretical Part

1.1. Biocompatible polymers

The earliest known evidence of using artificial materials as tooth replacements dates back to the 2nd and 6th centuries AD[1, 2], respectively. However, the systematic introduction of artificial tools into the human body for treating diseases or health disorders began only about 70 years ago. Today, a wide range of materials is utilized in various medical applications, with polymer science serving as a crucial link between material science and life sciences.[3] Additionally, a plethora of new, well-defined nano-objects made from polymers are being developed for biomedical purposes. As a result, self-assembled nanostructures based on biocompatible polymers are being intensively studied, leading to new approaches not only for targeted treatments[4, 5] but also for diagnostics. [6, 7]

The production of polymeric materials for the medical industry increases every year, with the global biomaterials market size estimated at USD 106.5 billion in 2019.[8] This market includes materials used in cardiovascular medicine (stents, guidewires, vascular grafts), ophthalmology (synthetic corneas, intraocular and contact lenses), dentistry and orthodontics (tissue regeneration materials, dental membranes), orthopedics (joint replacement biomaterials, bioresorbable tissue fixation products, viscosupplementation, spine biomaterials), wound healing, tissue engineering, plastic surgery, neurology, and more. [8]

Of particular interest are biocompatible polymers—polymeric materials that do not produce toxic or immunological responses when exposed to the body. These materials can be either natural or synthetic in origin. They are often categorized into groups based on their solubility in water (soluble vs. insoluble) or according to specific properties essential for their intended use, such as degradability or conductivity. The structures of the most relevant biocompatible polymers for this work are shown in **Figure 1**.

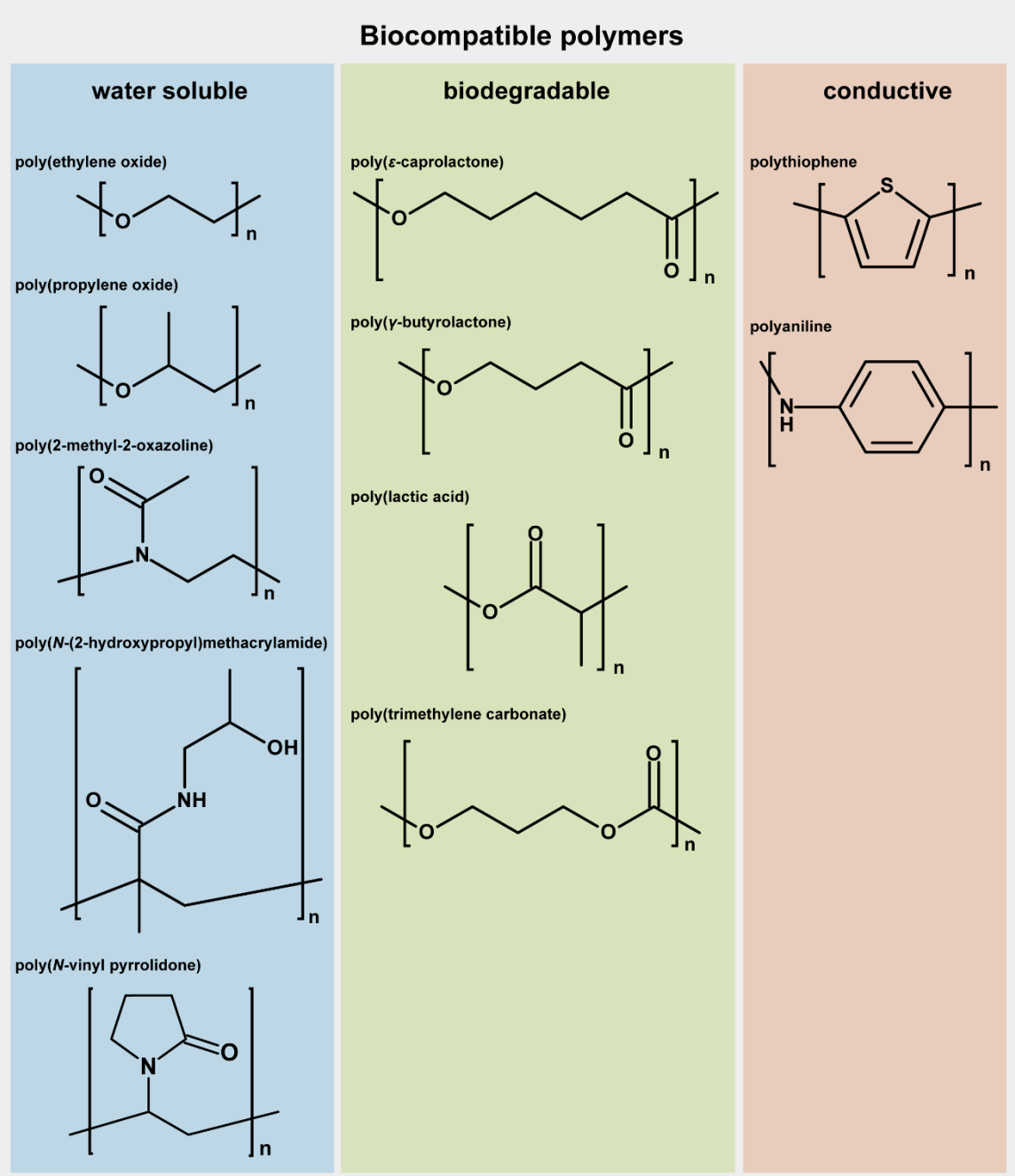

Figure 1: Examples of biocompatible polymers.

1.1.1. Water-soluble polymers

Poly(ethylene oxide) (PEO), also commonly referred to as poly(ethylene glycol) (PEG), has become widely used in many commercial applications.[9] PEO is particularly valued in medical applications due to its solubility in both water and organic solvents, and its hydroxyl end groups can be easily modified. Once functionalized, water-soluble PEO can be conjugated to drugs to extend their pharmacokinetic profiles, a process known as PEGylation.[10, 11] A structurally similar polymer, poly(propylene oxide) (PPO), shares many properties with PEO, but its solubility

decreases significantly as its molar mass increases. As a result, PPO is often combined with PEO in block copolymers, which function as excellent surfactants.[12]

Despite the promising applications of PEO in medicine, concerns about its biocompatibility have arisen. Studies suggest that the intensive use of PEO may lead to potent immunogenicity, and widespread use of PEO-based nonionic surfactants in everyday products such as soaps, shampoos, and cleaners has contributed to the presence of anti-PEO antibodies in a significant portion of the Western population.[13, 14] Consequently, alternatives have been sought, and water-soluble polyoxazolines, particularly poly(2-methyl-2-oxazoline) (PMeOx) and poly(2-ethyl-2-oxazoline) (PEtOx), have gained attention.[15, 16] These polymers are easily produced through the cationic ring-opening polymerization (ROP) of 2-alkyl-2-oxazolines. The polymerization scheme for this chain-growth process is illustrated in **Figure 2**. Hydrophilic materials are obtained when methyl (PMeOx) or ethyl (PEtOx) groups are present at the position labeled "R" in the scheme.

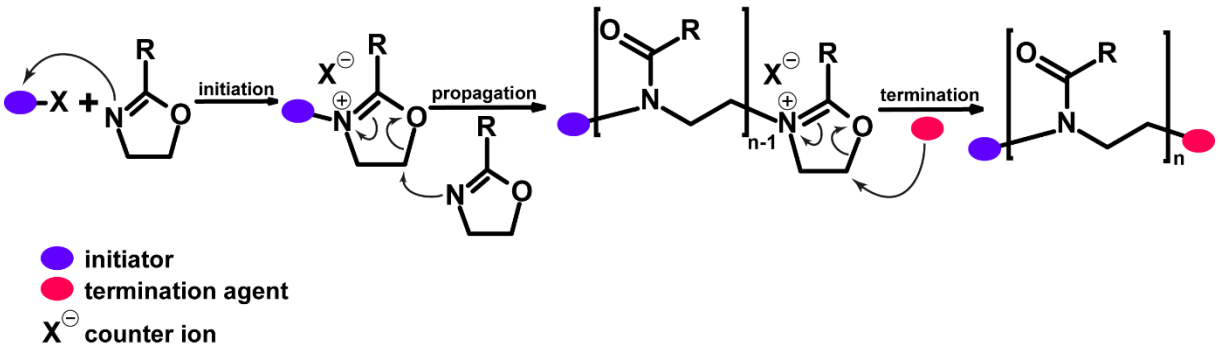

Figure 2: Mechanism of cationic ROP of oxazolines.

It is also noteworthy that telechelic polyoxazolines can be produced by selecting appropriate initiators (shown in purple in **Figure 2**) and termination agents (shown in pink in **Figure 2**). This allows for a wide range of post-polymerization modifications to meet specific needs. Compounds with excellent leaving groups, such as aliphatic brominated hydrocarbons or organic tosylates or triflates, are typically used as initiators. It is crucial to avoid moisture during polymerization, and the polymer chain can be terminated by an intentionally added nucleophile.[17]

Another important biocompatible, water-soluble polymer is poly(*N*-(2-hydroxypropyl)methacrylamide) (PHPMA, structure shown in **Figure 1**), which is produced through controlled free radical polymerization of *N*-(2-hydroxypropyl)methacrylamide. This well-documented polymer is frequently used in nanomedicine.[18] In addition to copolymerization with suitable functional comonomers, PHPMA can be easily modified due to the hydroxyl groups

along its polymer chain, offering opportunities for tailored applications such as polymer-drug conjugates, imaging polymers, nanoaggregates, micelles, and polymerosomes.[19, 20]

N-vinylpyrrolidone is another monomer capable of undergoing controlled free radical polymerization to produce a water-soluble polymer known as poly(*N*-vinylpyrrolidone) (PVP, structure shown in **Figure 1**. Like other water-soluble polymers, PVP is being studied for various applications, depending on the specific arrangements and modifications of its molecular chains.[21] Additionally, the brown complex formed by PVP with iodine is widely used in surgical procedures as a disinfectant for the skin.[22]

1.1.2. Biodegradable polyesters

Aliphatic polyesters represent the largest group of biodegradable polymers today.[23] These compounds are primarily sourced through either biotechnological production by bacteria or conventional chemical synthesis.

Bacterial aliphatic polyesters are mainly represented by polyhydroxyalkanoates (PHAs). While PHAs degrade effectively in the presence of certain microorganisms with active esterases, their biodegradability in human tissue remains questionable due to the lack of specific enzymes. The most well-known PHAs are poly(3-hydroxybutyrate) (PHB) and poly(3-hydroxyvalerate) (PHV). Additionally, copolymers can be produced depending on the bacterial species and growth conditions. The general chemical structure of PHAs is illustrated in **Figure 3** (PHB when R = methyl group, PHV when R = ethyl group).

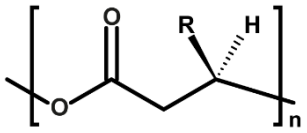

Figure 3: General formula of polyhydroxyalkanoates PHB if R = -CH_3, PHV if R = -C_2H_5).

Beyond biotechnological production, chemical synthesis is also of great interest, particularly the ring-opening polymerization (ROP) of lactones, which allows for the production of polymers with desirable molar masses and narrow dispersity.[24] A wide range of catalysts can be used, as ROP of lactones can proceed via three different mechanisms: anionic, cationic, and coordination-insertion.[25] In some cases, ROP can be initiated by heating alone. Additionally, isolated enzymes, most often lipases, can convert lactones into low-molecular-weight polyesters.

Biodegradability is a highly valued property of these compounds. The ester bonds in the polymer backbone undergo slow hydrolytic scission, with the reaction rate dependent on various material properties, including monomer structure, molar mass, hydrophobicity, crystallinity, phase

microstructure, and material processing.[26] Moreover, human esterases, particularly lipases, can selectively cleave ester bonds, accelerating the degradation process. As a result, these materials have found widespread use in medical applications, such as surgical sutures.[27]

Polymer erosion

There are two main mechanisms of polymer degradation: bulk erosion and surface erosion. Bulk erosion occurs when the material degrades uniformly throughout its entire volume, whereas surface erosion is characterized by a significantly higher degradation rate at the surface. While most materials experience both forms of degradation, one mechanism typically dominates.[28]

As mentioned earlier, polyesters undergo both hydrolytic and enzymatic degradation. Generally, hydrolytic degradation of polyesters tends to follow the bulk erosion mechanism, while enzymatic degradation proceeds more by surface erosion. Understanding these mechanisms allows for the design of material structures tailored to specific applications.[29]

Enzymatic degradation is inherently dependent on the activity and substrate specificity of the respective enzymes. There is a significant difference between intracellular and extracellular esterases, with relatively higher lipase activity found in lysosomes within the intercellular space. These lipases tend to fuse with vesicles formed by phagocytosis and endocytosis, where the vesicle contents are digested by lysosomal enzymes.

This natural phenomenon can be considered when developing new drug delivery strategies or enhancing pharmacokinetics.[28, 30]

1.1.3. Conductive polymers

Conductive polymers exhibit significant electrical (semi)conductivity, making them vital in various applications. Examples of conductive polymers include polythiophene and polyaniline, whose structures are shown in **Figure 1**, as well as polyacetylene, polypyrrole, and poly(p-phenylene). The key to their electrical conductivity lies in the system of conjugated bonds, along with the presence of mobile charge carriers, such as electrons and holes.[31] It has been demonstrated that polymeric materials with varying levels of conductivity can be synthesized.[32-34] In **Figure 4**, the conductivities of different conventional materials are compared with those of conductive polymers.

One of the most important characteristics shared by conductive polymers and conventional inorganic semiconductors is their ability to increase conductivity through doping. However, doping organic polymers involves the partial oxidation or reduction of the polymeric chain. Each oxidation state of a specific polymer exhibits a characteristic reduction potential. For instance, in

doped polyacetylene, shown in **Figure 4**, dopants such as iodine, lithium, silver perchlorate, and others have been successfully used.[35] It has been established that using specific dopants can increase the conductivity of certain polymers by several orders of magnitude.

Another example is protonated polyaniline, which highlights the importance of doping in achieving conductivity in organic polymers. The non-protonated form of polyaniline exhibits such low conductivity that it is considered an insulator.

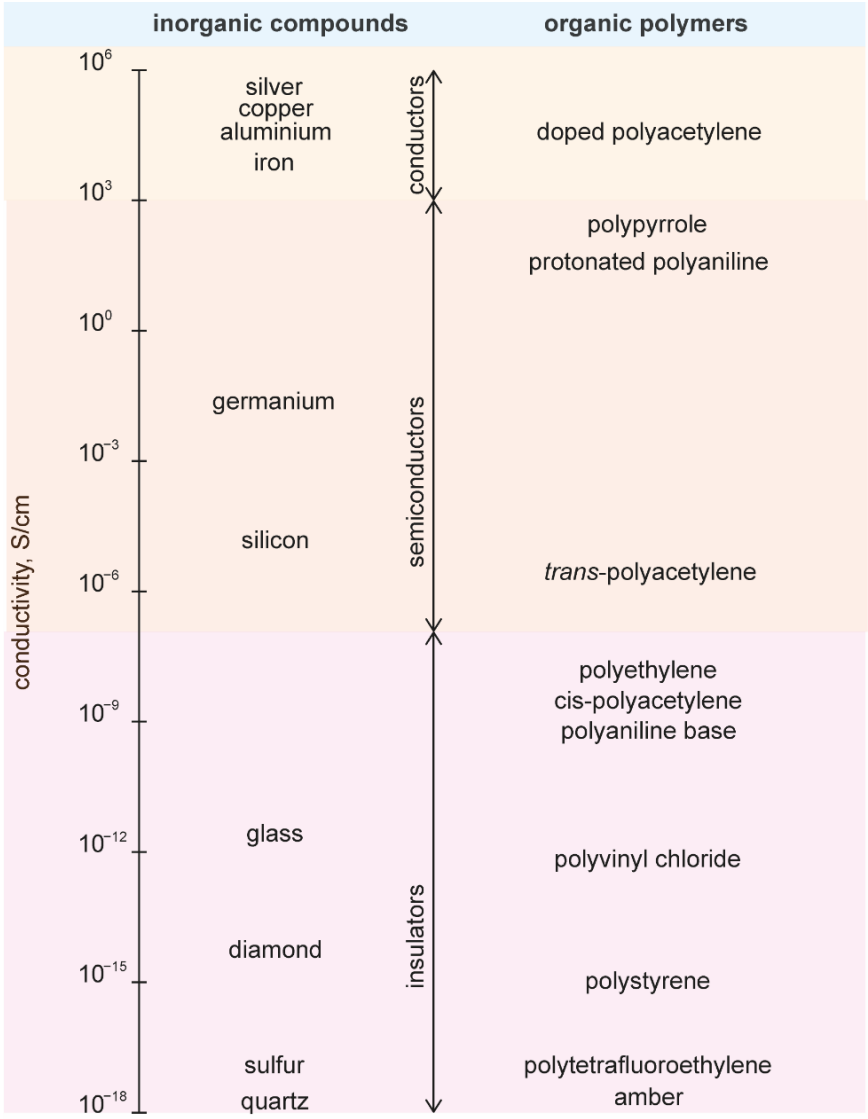

Figure 4: Comparison of conductivity between inorganic compounds and organic polymers.[31] In summary, conductive polymers have expanded the range of semiconductor materials used in electronics, including applications such as sensors.[36]

1.2. Polymer architectures

There are numerous ways to modify the chemical structure and topology of polymers to achieve desired properties in the final product. This is a crucial task for polymer scientists, who

continually seek to discover optimal solutions for specific applications. Generally, these properties can be adjusted through copolymerization, where two or more monomers are combined, leveraging the strengths of each homopolymer. Additionally, the properties can be finely tuned by employing various copolymerization strategies. The most common copolymer structures are shown in the upper part of **Figure 5**. It is important to note that even when the chemical composition of two linear copolymers is identical, the arrangement of repeating units can significantly influence the material's final properties.[37]

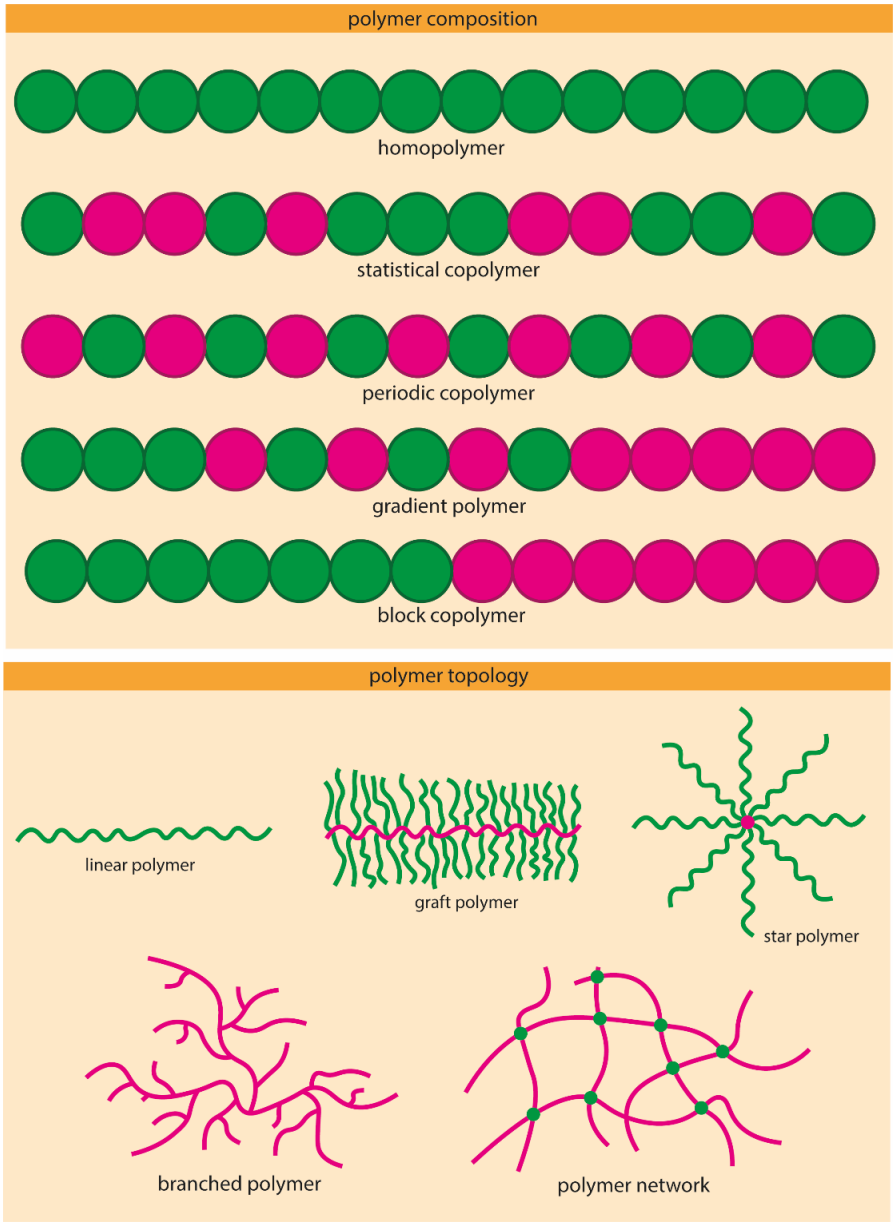

Figure 5: Common copolymer architectures.[38, 39]

Polymer structures can be further modified by introducing a node where three or more chains converge. The most common polymer architectures that meet this criterion are depicted in the lower part of **Figure *5***. This approach can significantly alter material properties. For instance,

viscosity, a critical property, changes with the number of nodes in a polymer's architecture. As the number of branches increases in a polymer structure with the same overall molecular weight, the viscosity of the solution or polymer melt decreases.[40]

There are three main types of polymer architecture: linear, branched, and network architectures, each with several subtypes, as shown in **Figure *5***. For example, the properties of a linear polymer can be easily modified by changing its molar mass. This is evident when comparing industrially produced high-density polyethylene (HD-PE, 200-500 kDa) with ultra-high-molecular-weight polyethylene (UHMWPE, 4-6 MDa). Due to its higher molar mass, UHMWPE has a very low coefficient of friction and high mechanical strength, making it ideal for use in orthopedic joint replacements.[41] In general, linear polymers tend to have higher densities and melting points compared to branched polymers. Polymer networks, which have complex 3D structures, cannot be characterized by molar mass but rather by crosslink density. Networks with high crosslink density are rigid, while those with low crosslink density are known for their swelling behavior, and when swollen with water, they are referred to as hydrogels.

The author of this thesis has summarized the most widely used strategies for polyesters in a review article, which is included in the **Appendix 1**.[38]

1.2.1. Block copolymers

Among the various types of designed polymer structures, block copolymers stand out as exceptional tools for combining entirely different polymers to create new materials with unique properties. Block copolymers consist of two or more chemically distinct and often immiscible segments, or "blocks," that are covalently bonded together.[42]

There is also an intermediate structure between random copolymers and block copolymers, known as gradient copolymers. The structural differences between these types are illustrated in **Figure *5***. In gradient copolymers, the glass transition temperature breadth changes significantly. Unlike block copolymers, which typically display two distinct peaks in differential scanning calorimetry (DSC) spectra, gradient copolymers exhibit a single broadened peak.[43] Additionally, gradient copolymers tend to have a higher critical micelle concentration (CMC) compared to block copolymers with the same chemical composition.[44]

1.3. Self-assembled polymeric systems

Self-assembly is a phenomenon in which an initially disordered system of polymer chains spontaneously organizes into a well-ordered structure due to local noncovalent interactions among the components or between the components and the solvent. The strengths of these

noncovalent interactions are listed in **Table 1** and compared to the typical values for covalent bonds.[45]

Table 1: Energy of different types of chemical bonds and interactions.[45]

Bond/interaction	**Energy (kJ·mol^{-1})**
Covalent bond	100-400
Ion-ion interaction	200-300
Ion-dipole interaction	50-200
Dipole-dipole interaction	5-50
Hydrogen bond	4-120
Cation-π interaction	5-80
π-π interaction	0-50
Van der Waals interaction	< 5
Hydrophobic effect	entropy driven

Supramolecular chemistry, the field that studies these self-assembling processes, is relatively new, with its conceptual foundation established in the 1960s. During that time, chemists from various disciplines began exploring how molecules interact with their surroundings and with each other, leading to systematic research in this area. This research has attracted not only (bio)organic chemists and general and physical chemists but also material scientists, particularly those focusing on the self-assembly of specific polymers.[46]

Self-assembled systems are ubiquitous in nature and gain functionality through hierarchical organization. Notable examples include cytoplasmic membranes and the formation of virions. These natural systems have inspired a wide range of scientists interested in biomimetics and bionics.[47]

Focusing on man-made polymeric self-assembled structures, several important nanostructures can be easily prepared. These structures are generally classified into 3D nanoobjects (e.g., nanoparticles, micelles, polymerosomes), 2D nanoobjects (e.g., nanofilms, bilayers), and 1D objects (e.g., nanofibers, nanotubes). The unique self-assembly of these supramolecular structures is often driven by the amphiphilic properties of the molecules, as well as their specific structure and geometry.

The final shape of these self-assembled structures is commonly predicted using the critical packing parameter (C_{PP}), which is defined by **Equation 1** and the value predicts the aggregate morphology:

$$C_{PP} = \frac{V}{A \cdot l_c} \tag{1}$$

where:

- V is the effective volume occupied by the hydrophobic chain,
- A is the effective hydrophobic headgroup surface area,
- l_c is the maximum effective length of the molecule.

When the critical packing parameter C_{PP} is less than 1/3, the structure typically forms a spherical micelle. As C_{PP} increases to between 1/3 and 1/2, the structure usually transitions to a cylindrical micelle. When C_{PP} falls between 1/2 and 1, a bilayer vesicle is formed. As C_{PP} approaches 1, the structure tends to become lamellar. If C_{PP} exceeds 1, the formation of inverse micelles is likely.[45] The typical shapes corresponding to these C_{PP} values are shown in **Figure 6**.

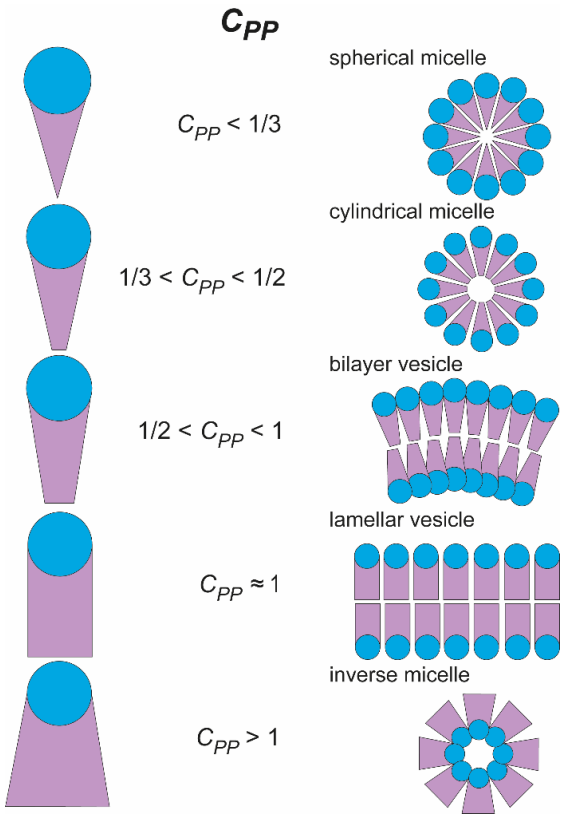

Figure 6: Relationship between molecular shape and resulting supramolecular structure.[48]

1.4. Characterization methods of self-assembled polymeric systems

The complexity and heterogeneity of the self-assembly phenomenon require detailed structure analysis, as evident in the experimental part. Below, the selected methods are discussed more in detail.

1.4.1. Scattering methods

Scattering methods are essential for studying nanoscale materials, providing critical insights into their structure, size, shape, and properties. These techniques exploit the interaction between electromagnetic waves and matter, particularly effective when the particle size is comparable to the wavelength of the radiation used. Light, X-rays, and neutron beams are commonly employed in these methods, each offering unique information about the material. Light scattering, in particular, is useful for analyzing particle size, shape, and molecular weight, while X-ray and neutron scattering reveal detailed internal structures. These methods are vital tools in materials science, biology, and nanotechnology, enabling a deeper understanding of the nanoscale world.[49]

1.4.1.1. Static light scattering (SLS)

In macromolecular solutions, light scattering intensity increases compared to pure solvent due to additional local optical inhomogeneities given by the presence of polymer molecules. The intensity of scattered light is influenced by factors such as molecular weight, concentration, and the refractive index increment, which together determine the scattering behavior of the solution.[50]

To simplify the analysis, the Rayleigh ratio R_θ is introduced, which accounts for the intensity of scattered light, the distance from the detector, and the properties of the solution. This ratio is essential for interpreting light scattering data and is particularly useful for studying diluted solutions of small macromolecules, enabling the determination of molecular weight and solution behavior through scattering experiments. The relationship is mathematically expressed by the following **Equation 2**:

$$R_\theta = \frac{I_\theta \cdot r^2}{I_0 \cdot (1 + cos^2\theta)} = \frac{K \cdot c}{\frac{1}{M} + 2 \cdot A_2 \cdot c} \quad (2)$$

where:

- R_θ is the Rayleigh ratio, representing the intensity of light scattered by the solution relative to the incident light,
- I_θ is the intensity of light scattered at an angle θ,
- r is the distance from the detector to the sample,

- I_0 is the intensity of the incident light beam,
- K is the optical constant, defined as:

$$K = \frac{2 \cdot \pi^2 \cdot {n_0}^2}{N_A \cdot {\lambda_0}^4} \cdot \left(\frac{\delta n}{\delta c}\right)^2 \quad (3)$$

where:

- n_0 is the refractive index of the solvent,
- N_A is Avogadro's number,
- λ_0 is the wavelength of light in a vacuum,
- $\delta n/\delta c$ is the refractive index increment, indicating how the refractive index changes with concentration,

- c is the concentration of the solute (macromolecules) in the solution,
- M is the molar mass of the macromolecules,
- A_2 is the second virial coefficient, which accounts for interactions between macromolecules in the solution.

When large particles are present in a solution, light scattering becomes more complex due to intramolecular interference, which causes the scattered light to vary significantly with the angle of observation. This angular dependence requires the introduction of a form factor P_θ to accurately describe the scattering pattern, as expressed in **Equation 4**:

$$P_\theta = \frac{R_\theta}{R_0} \quad (4)$$

where:

- R_θ is the Rayleigh ratio at a specific scattering angle θ,
- R_0 is the Rayleigh ratio extrapolated at θ=0°, where there is no interference and the scattering is isotropic.

The Rayleigh ratio R_θ is no longer uniform and depends on both the size and shape of the particles. As the particle size increases, the scattering intensity and interference patterns become more pronounced, necessitating more detailed calculations to determine parameters such as the radius of gyration. These factors make the analysis of large particles more intricate compared to smaller

ones. Despite these complexities, this type of measurement can still be valuable for characterizing larger particles, such as nanoparticles.[49, 50]

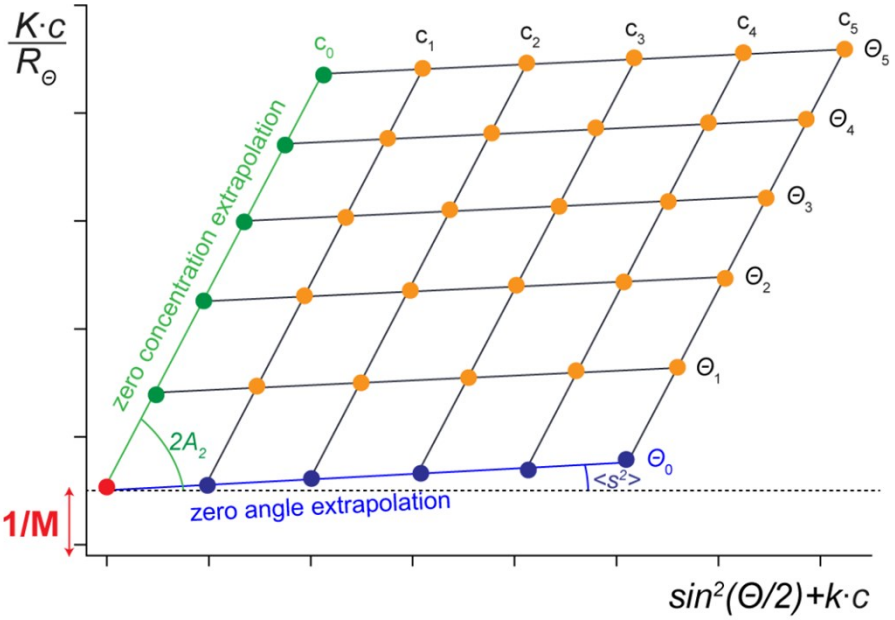

Figure 7: Zimm Plot: Yellow dots represent the measured data points, blue dots indicate the extrapolation to zero angle, green dots show the extrapolation to zero concentration, and the red dot marks the intercept at zero angle and zero concentration.[49]

The Zimm plot shown in **Figure 7** is a graphical method used in static light scattering to determine key properties of macromolecules and nanoparticles in solution, such as molecular weight M, the second virial coefficient A_2, and the mean square radius of gyration R_g. By plotting the scaled scattering intensity $\frac{K \cdot c}{R_\theta}$ against the combined variable $sin^2\left(\frac{\theta}{2}\right) + k \cdot c$, where k is an adjustable parameter, and performing a double extrapolation to zero angle and zero concentration, these properties can be extracted. The intercept at zero angle and concentration provides the molecular weight M, the slope at zero angle gives the second virial coefficient A_2, and the slope at zero concentration yields the mean square radius of gyration R_g. This plot is crucial for characterizing the size, shape, and interaction behavior of polymers and nanoparticles in solution, making it a versatile tool in the study of various particulate systems.

1.4.1.2. Dynamic light scattering (DLS)

Another light scattering technique used to determine particle size is dynamic light scattering (DLS), often referred to as Quasi-elastic light scattering (QELS) due to its reliance on nonelastic scattering. This method is widely employed for the detection and characterization of nanoparticles in solution or colloidal suspension, making it particularly valuable in supramolecular science.

The principle of DLS is based on the fact that larger particles move more slowly than smaller ones when considering only Brownian motion. When the light scatters off particles at two different time intervals, the distances to the detector vary, leading to fluctuations in the intensity of the scattered light. These intensity fluctuations are slower for larger particles and faster for smaller particles. By analyzing these fluctuations using autocorrelation, the time autocorrelation function can be determined, which indicates how quickly the intensity changes occur. Once the autocorrelation function is known, the diffusion coefficient D of the dispersed particles can be calculated. For spherical particles, the hydrodynamic diameter D_H can be determined using the following **Equation 5**:

$$D_H = \frac{\mathrm{k} \cdot T}{3\pi \cdot \eta_0 \cdot D} \tag{5}$$

where:

- k is the Boltzmann constant,
- T the temperature,
- η_0 the viscosity of the solvent.

DLS can also be applied to nonuniform systems, although interpreting of the autocorrelation function is more complex in these cases. However, the average value of D_H and its dispersity can still be determined. For uniform systems, the dispersity of D_H is equal to zero.

Additionally, combining results from SLS and DLS, provides further insight into particle topology. The ratio of radius of gyration R_g and hydrodynamic radius R_h offers a rough estimate of particle shape. **Table 2** summarizes the typical R_g/R_h ratios for different particle morphologies:

Table 2: The particles' morphologies and their typical R_g/R_h ratios.[49]

topology	$\boldsymbol{R_g/R_h}$ **ratio**
homogenous sphere	0.775
hollow sphere	1
ellipsoid	0.775 – 4
random polymer coil	1.505

In the context of DLS, zeta potential is a critical parameter that provides insight into the stability of colloidal dispersions. Zeta potential quantifies the electrostatic potential at the slipping plane

of particles, which is crucial for understanding their stability and interactions within the dispersion. The zeta potential arises from the electrical double layer surrounding the particles, which consists of a charged layer adjacent to the particle surface and a diffuse layer extending into the surrounding medium. High absolute values of zeta potential, either positive or negative, generally indicate a strong electrostatic repulsion between particles, suggesting enhanced stability and reduced propensity for aggregation. Conversely, low zeta potential values imply weaker electrostatic interactions, which can lead to particle agglomeration and system instability. Therefore, while DLS provides valuable information on particle size, incorporating zeta potential measurements offers a more comprehensive assessment of the colloidal system's stability and behavior, aiding in the formulation and optimization of various nanoparticle-based applications.[49, 51]

1.4.1.3. Scattering of X-rays and neutrons

The X-rays are well-known for their use in analyzing materials with crystalline structure, but they can also be effectively employed in the study of colloidal dispersed systems. The primary difference between light and X-ray scattering lies in their wavelengths, leading to distinct interactions with matter. The higher frequency of X-rays allows them to scatter off electrons, providing higher resolution. Compared to light scattering, X-ray scattering offers several advantages including the ability to determine not only molar mass M, the second virial coefficient A_2 and radius of gyration R_g, but also additional geometrical parameters that more precisely describe the shape of dispersed particles. Additionally, X-ray scattering can be used to analyze optically nontransparent samples.

The Small-Angle X-ray Scattering (SAXS) is the most commonly used technique for measurements of colloidal solutions. In SAXS, scattered X-rays are detected at very small angles, typically within a few angular minutes, enabling the examination of particles with dimensions ranging from 1 to 100 nm.[52]

Neutron scattering shares many similarities with X-ray scattering. However, unlike X-rays, neutrons do not scatter off electrons but interact with atomic nuclei. Therefore, the nuclear properties of the sample are crucial, characterized by neutron scattering coherent length, often referred to simply as the scattering length B. There is a significant difference in B between protium on one side, and deuterium and other atoms commonly found in soft matter (C, N, O). By combining non-deuterated and deuterated materials, the contrast between components of the system can be varied, allowing for a detailed description of the structure of investigated particles such as hydrophobic cores and hydrophilic coronas. Moreover, neutron scattering does not require very diluted solutions. The instrumentation is similar to SAXS and is known as Small-Angle

Neutron Scattering (SANS). However, due to the need of a sufficiently intense neutron source (typically a nuclear reactor), this method is less widely available.[52]

1.4.2. Asymmetric flow field flow fractionation (A4F)

Asymmetric flow field flow fractionation (A4F) is a widely used separation and characterization technique for nanoparticles, offering several advantages over traditional methods like size exclusion chromatography (SEC). Unlike SEC, which relies on a stationary phase to separate macromolecules, A4F utilizes a vertical flow of liquid to achieve separation. In A4F, particles are separated based on their size and diffusion coefficients; smaller particles with higher diffusion coefficients are detected earlier than larger ones. This method is particularly effective for detecting and analyzing particles in a broader range of dimensions, making it a powerful tool in nanoparticle research.

1.4.3. Electron microscopy

Scanning Electron Microscopy (SEM) and Transmission Electron Microscopy (TEM) are powerful analytical techniques that utilize the properties of electrons to image very small objects. Unlike classical optical microscopy, which uses photons for imaging, SEM and TEM use electrons, allowing for much higher resolution due to the shorter wavelength of electrons compared to light. This results in magnifications that can reach up to 10 million times[53], making these techniques particularly useful for imaging nanoscale objects.

Despite both SEM and TEM employing electrons for imaging, they differ significantly in their methods. SEM creates images by detecting electrons scattered from the surface of a sample, producing detailed images of the surface morphology. In contrast, TEM detects electrons that pass through the sample, allowing for the visualization of internal structures or layers beneath the surface. As a result, sample preparation differs between the two techniques: SEM samples are typically coated with a conductive material (such as gold, platinum, osmium, or graphite) to enhance electron scattering, while TEM samples require the preparation of extremely thin sections to allow electrons to transmit through the sample for imaging.[54, 55]

1.5. Polymer sensors

The field of polymer sensors and actuators is one of the most cutting-edge areas of current research.[56, 57] These devices rely on materials with specific properties that change in response to external stimuli, which can be either physical or chemical. These changes may be reversible or irreversible.[57] The most common stimuli for polymer sensors include pH, ion concentration, non-charged molecules, radiation, temperature, mechanical force, and electric or magnetic fields.

1.5.1. pH sensors

The glass electrode is the most widely used pH sensor due to its sensitivity, reliability, and versatility, making it essential for precise pH measurements across various fields. However, in certain applications where conventional pH meters or indicators are impractical, polymer-based pH sensors have become increasingly important. These sensors, which often involve materials with pH-dependent protonation or deprotonation, can be applied on small scales, such as thin films around 10 μm thick. For example, hydrogels based on poly(2-hydroxyethyl methacrylate-co-2-dimethylaminoethyl methacrylate) have demonstrated high sensitivity to proton concentration, with sufficient accuracy for various applications.[58] Additionally, other acrylate derivatives have shown promise in expanding the capabilities of these polymer-based pH sensors, highlighting their importance alongside traditional glass electrodes in pH-sensitive environments.[59]

1.5.2. Chemoselective sensors

Polymer-based chemoselective sensors are designed to detect specific analytes, including ions, uncharged compounds, and bioactive molecules, with high precision. These sensors utilize chemoselective reactions to enhance their specificity and sensitivity. By incorporating functional groups or molecules that selectively react with the target analyte, these sensors can produce measurable signals, often electrical or optical, upon detection.[57]

Chemoselective reactions play particularly a crucial role in developing functional protein-based sensors by enabling precise modifications that enhance performance and specificity. Reactions such as bioorthogonal chemistry, thiol-ene reactions, and enzyme-mediated modifications allow the selective attachment of signaling molecules to proteins without disrupting their native functions. This precision is essential for creating highly sensitive and specific sensors used in medical diagnostics, environmental monitoring, and industrial applications. By tailoring chemoselective modifications, protein-based sensors can accurately detect a wide range of analytes, making them invaluable tools across various fields.[60, 61]

1.5.2.1. Ion-selective sensors

Materials used for ion-selective sensors are often made from conductive polymers, enabling signal detection potentiometrically or conductometrically after stimulus. This approach has been extensively studied for medical applications, particularly as real-time concentration detectors.[62, 63] For example, a calcium-selective electrode was created from polyaniline, which was further functionalized with bis-[4-(1,1,3,3-tetramethylbutyl)phenyl]phosphate, a key component known as an ionophore. Ionophores, such as valinomycin, nystatin, or natamycin, are compounds that increase the permeability of biological membranes to specific ions.[64] Typically, they have a

hydrophobic part that anchors into the lipid bilayer and a hydrophilic part responsible for ion-ionophore interaction, facilitating ion transfer across the membrane. In analytical chemistry, selective ionophores are crucial for constructing ion-selective electrodes.

Another widely used natural ionophore is porphyrin. Heme, a prosthetic group in all hemoproteins, consists of a tetrapyrrole core with a ferrous cation at its center. This metal ion-porphyrin interaction has inspired the development of man-made sensors for engineering and electronics, as porphyrins are effective at transforming changes in physical and chemical parameters into electrical signals.[65, 66]

1.5.2.2. Gas sensors

Gas sensors, particularly those used in electronic noses (e-noses), have seen significant advancements over recent decades. These sensors, including types like metal oxide semiconductor, electrochemical, and conducting polymer sensors, are crucial for detecting and identifying gases and odors. The compact design of modern e-noses, which integrates small, efficient sensor arrays and advanced microprocessors, has broadened their application range from food quality assessment to environmental monitoring and medical diagnostics. The development of portable, low-power e-noses has made it possible to detect gas leaks, monitor air quality, and even diagnose diseases through breath analysis, demonstrating the versatility and importance of these sensors in various fields.[67]

For example, Professor Stejskal's team demonstrated that a printed, modified polyaniline sensor could detect ammonia at concentrations as low as 500 ppb, showcasing its extreme sensitivity.[68] Additionally, sensors have been developed for detecting humidity, nitrogen dioxide, and various other gases.[67, 69]

1.5.2.3. ROS sensitive detectors

Reactive oxygen species (ROS) are highly reactive molecules that play dual roles in biological systems, both in normal cellular signaling and in causing oxidative damage under pathological conditions. Detecting and quantifying ROS is crucial for understanding their role in oxidative stress and disease, particularly in conditions like cancer, inflammation, diabetes, and neurodegenerative disorders.[70] However, the detection of ROS is challenging due to their short lifespan, low steady-state concentrations, and rapid reactivity. To address this, various sensors, including fluorescent and electrochemical probes, have been developed to monitor ROS, such as hydrogen peroxide, superoxide anion, hydroxyl radicals, and hypochlorite. Fluorescent probes offer real-time monitoring in living cells and are highly sensitive, though they can be limited by issues such as photobleaching and probe stability.[71]

In contrast, electrochemical methods provide a robust alternative, especially when enhanced with biological catalysts like superoxide dismutase or synthetic biomimetic enzymes. These methods allow for precise detection of ROS at very low concentrations, making them invaluable tools in medical diagnostics and research on oxidative stress-related conditions. By utilizing these advanced sensing techniques, a deeper understanding of the roles of ROS in cellular processes and disease progression can be gained.[72]

1.5.3. Temperature-responsive polymer sensors

Temperature-responsive polymers are materials that undergo significant and discontinuous changes in their physical properties when exposed to temperature variations, often affecting their solubility in a given solvent. The most common behavior observed in these polymers is the Lower Critical Solution Temperature (LCST), below which the polymer is soluble in water, and above which it precipitates. Less commonly, some polymers exhibit an Upper Critical Solution Temperature (UCST), where they are soluble above a certain temperature and precipitate below it.[73]

These polymers are widely used in various fields, including drug delivery, tissue engineering, and bioseparation, because of their ability to respond to small changes in temperature. For instance, thermoresponsive surfaces can be used in tissue engineering to control cell adhesion or release by simply adjusting the temperature. In drug delivery, these polymers enable controlled release of drugs in response to body temperature. Additionally, they play a role in chromatography, allowing for temperature-controlled separation processes.[74, 75]

Temperature-responsive polymer sensors specifically utilize these materials, which exhibit LCST behavior, to detect changes in temperature. Often, these sensors are composed of copolymers made from monomers like *N*-isopropylacrylamide, *N*-isopropylmethacrylamide, *N*-propylacrylamide, or *N*-*tert*-butylacrylamide, combined with a fluorescent dye. The dye's fluorescence changes as the polymer's solubility shifts in response to temperature changes, providing a clear indication of the temperature variation. This approach allows for highly sensitive and accurate temperature monitoring.[73, 76]

2. Aims of the thesis

Infectious diseases and inflammations pose significant challenges today, exacerbated by the increasing spread of antibiotic resistance. Motivated by these pressing issues, this thesis addresses these challenges in a comprehensive manner through the use of polymers. The research is divided into three primary objectives:

1. In the first part, polymers are utilized as the matrix for antibacterial drug-carrying nanoparticles (NPs) designed as a delivery system.

2. The second part focuses on using polymers to encapsulate insoluble antibacterial drugs, forming polymer-stabilized sub-micrometer particles intended for formulation.

3. In the third part, functional polymers are applied as a sensor layer on surfaces, rather than particles, to detect inflammations and infections.

These specific aims are detailed below.

2.1. Fine-tuning biorelevant properties of NPs

The first objective of this thesis is to synthesize and characterize block copolymers based on poly(ethylene oxide)-b-poly(ε-caprolactone) (PEO-b-PCL) and to modify the hydrophobic segment by incorporating a second monomer, γ-butyrolactone (γBL), to adjust specific biological properties, particularly enzymatic degradation. The introduction of γBL units into the hydrophobic block allows for fine-tuning the degradation rate, enhancing the versatility of these materials for biomedical applications. These modified copolymers are intended for use in the development of drug delivery systems, specifically for encapsulating and delivering the antibacterial antibiotic rifampicin. By varying the γBL content, the degradation behavior of the nanoparticles can be controlled, making them more suitable for specific therapeutic applications.

2.2. Enhancing biorelevant properties by polymeric surfactant stabilization

The second aim of this thesis is to investigate the self-assembly of the antimicrobial drug chloroxine and to achieve stable nanocrystalline particles through nanoprecipitation using polymeric non-ionic surfactants. This approach addresses the challenges posed by chloroxine's low solubility, aiming to enhance its biorelevant properties by stabilizing the particles in aqueous media. This formulation is designed to improve the antimicrobial efficacy of chloroxine while maintaining stability, making it a potential candidate for effective topical applications in treating skin infections.

2.3. Polymer based layer for selective potentiometric detection of ROS

The third aim of this thesis is the development of a polymer-based layer for a potentiometric sensor designed to detect reactive oxygen species (ROS) *in situ*, which are associated with inflammation. The sensor is constructed from a polymeric layer based on porphyrin cores linked by bis(thiophene) bridges. A metal ion is incorporated into the porphyrin core to enhance the sensor's selectivity and sensitivity. To prevent nonspecific adsorption of serum proteins, which could interfere with the sensor's function, the entire layer is shielded by a covalently bonded poly(2-methyl-2-oxazoline) (PMeOx) layer. This nonbiofouling coating ensures that the sensor remains functional in biological environments. The sensor responds potentiometrically to the presence of ROS, with its sensitivity designed to detect even the early stages of inflammation and infection. This innovative approach offers a promising tool for early diagnostics in biomedical applications.

3. Results and discussion

3.1. Biodegradable nanoparticles made of block copolymers

The block copolymer with hydrophilic and hydrophobic parts works well as a drug carrier, especially when the drug is significantly hydrophobic. It was shown that the core-shell nanoparticles are formed when this block copolymer with hydrophobic drug is nanoprecipitated. Poly(ethylene oxide)-*b*-poly(*ε*-caprolactone) is described as one of these copolymers for these purposes. In the previous work,[4] this copolymer was examined as a carrier for rifampicin, the relevant physicochemical properties and biological effects were described. As the data were analyzed, further research was done to adjust the nanoparticles disintegration which is the main goal of this branch of the thesis research and the result was published in the article shown in **Appendix 2**.

3.1.1. Block polymer design and synthesis

In the initial phase, the design and the synthesis of the drug carrier based on block copolymer composed of hydrophilic PEO and hydrophobic PCL were done as suggested by the scheme in the **Figure 8A**. This copolymerization was successfully done and described in the previously published article,[4] where the resulting block copolymer as a nanocarrier was equipped with the first-line antituberculotic agent – rifampicin with the entrapment efficiency between 14 to 30 %.

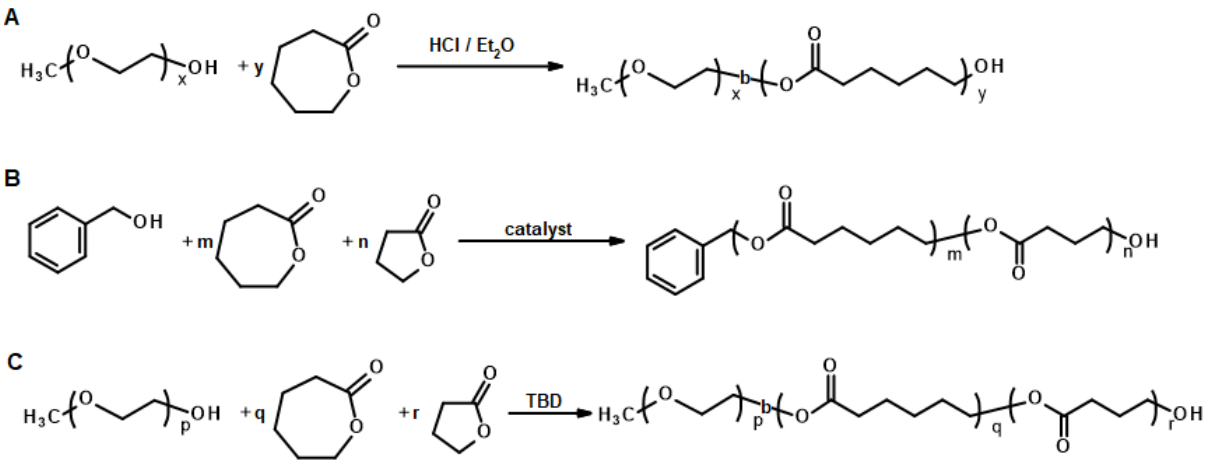

Figure 8: Polymerizations: Visualizing Chemical Reaction Schemes.[77]

Building on this achievement, the degradation rate of the copolymer has been taken in consideration as a possible feature for tailoring the micelle-like nanocarrier properties for adjusting the pharmacokinetics. The copolymerization *ε*CL with *γ*BL was selected as the method of determination the degradation rate.

In order to get control over the degradation rate, series of copolymers with various amounts of incorporated γBL in the polymer chain was needed to be synthetized. For this purpose, different copolymerization conditions were introduced and the results are as follows: the higher incorporation of γBL was observed when catalysts of anionic mechanism of the ring-opening polymerization were used. In addition, the higher the initial concentration of monomers in the solution, the higher the incorporation of γBL. It was also confirmed that using of nonpolar solvent contributes to the higher incorporation of γBL. All data were plotted in graphs, which are shown in **Figure 9**.

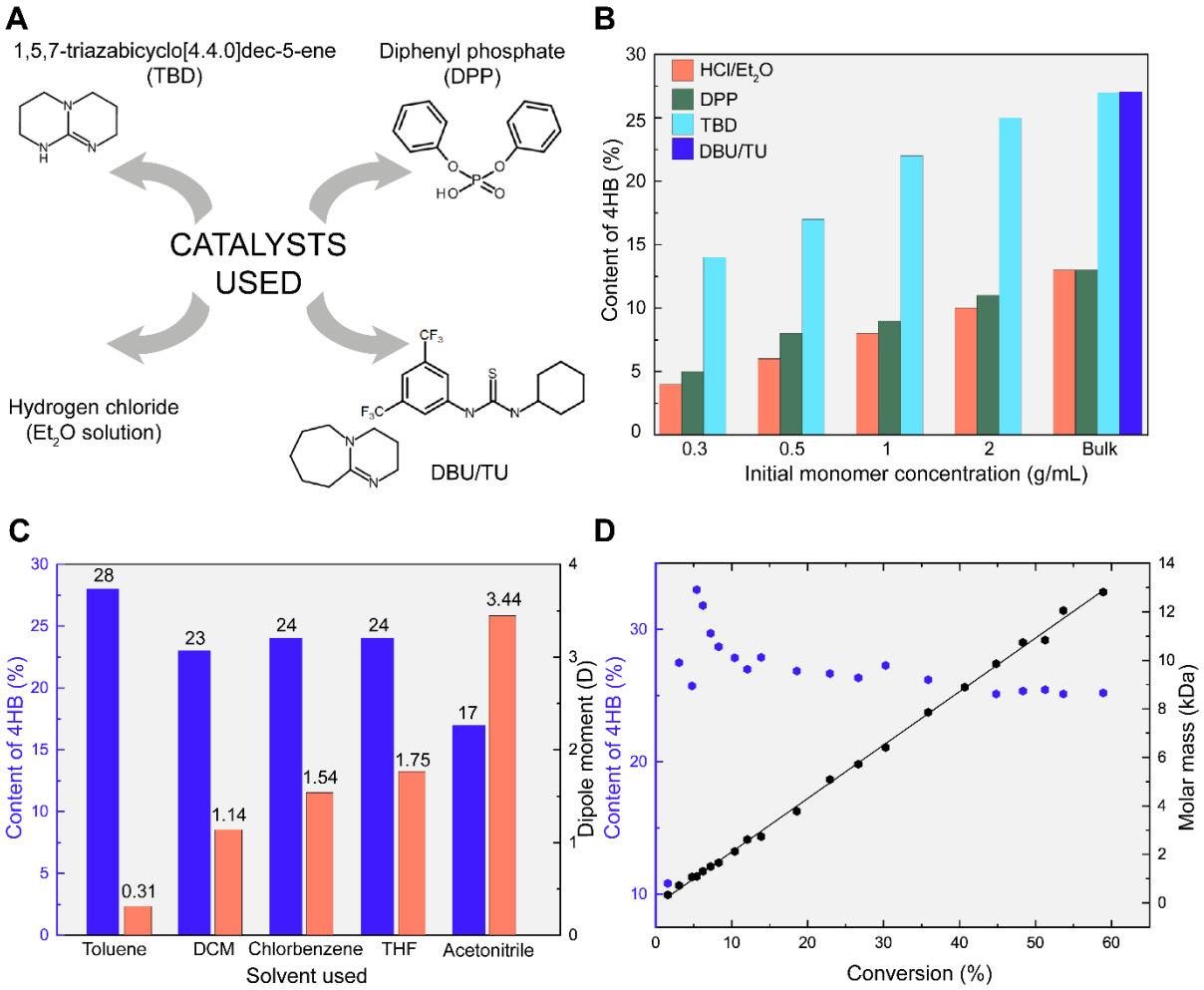

Figure 9: Optimization of copolymerization conditions. **A)** Various catalytical systems were tested to determine the 4HB content in the copolymers. **B)** The content of 4HB when various initial monomer concentrations and different catalytic systems were used and are listed in Table S2 in Supporting information.[77] **C)** Various solvents with different dipole moments were tested for the copolymerization using the most efficient catalytic system, TBD. **D)** The relationship between monomer consumption, the 4HB content in the polymer chain, and molar mass was investigated.[77]

3.1.2. Nanoparticles of block copolymers

With knowing about the incorporation of BL into the chain, five samples of block copolymers mPEO-b-(PCL-co-P4HB) with different molar masses and γBL ratios were synthesized by using commercially available macroinitiator poly(ethylene oxide) methyl ether, so there are two blocks in the polymeric chain, one hydrophilic and the second one hydrophobic (the specific hydrophobic ratios for each sample are provided in **Table 3**. The most efficient catalytical system of TBD was used in this case. All copolymers' characteristics are shown in **Table 3**. As evident from this table, sample B1 is the only one that does not contain P4HB, allowing its influence on selected biological properties (enzymatic degradation,…) to be examined. It can be also noted that two macroinitiators with molar mass 2 kDa (sample B2 and B3) and 5 kDa (sample B4 and B5) were used.

Table 3: Composition and characteristics of block copolymers.[77]

No.	Copolymer	HH-ratio[a)]	Yield [%]	$f_{\gamma BL}$[b)] [%]	$M_n^{NMRc)}$	$M_n^{SECd)}$	$Đ^{SECd)}$	CAC[e)] [μg mL^{-1}]	DACCA[f)] [μg mg^{-1}]
B1	$mPEO_{45}$-*b*-PCL_{81}	4.6	92	0	11 200	8300	1.21	9	20
B2	$mPEO_{45}$-*b*-(PCL_{39}-*co*-$P4HB_{13}$)	2.8	62	20	7500	6700	1.45	15	9
B3	$mPEO_{45}$-*b*-(PCL_{55}-*co*-$P4HB_{19}$)	4.0	60	21	9900	10 500	1.58	11	10
B4	$mPEO_{114}$-*b*-(PCL_{41}-*co*-$P4HB_{12}$)	1.1	63	18	10 800	7600	1.25	14	7
B5	$mPEO_{114}$-*b*-(PCL_{124}-*co*-$P4HB_{45}$)	3.6	59	21	23 000	12 300	1.61	10	4

[a)]The hydrophobic ratio was defined as (M_n, hydrophobic block)/(M_n, hydrophilic block), where the M_n of the hydrophilic block was held at either 2000 or 5000 depending on which macroinitiator was used; [b)]The polymer composition ratios of hydrophobic blocks were calculated using ^{1}H NMR data by dividing the integrated peaks of the repeating unit of γBL (δ 1.95 ppm) by the sum of the integrated peaks of γBL and εCL (δ 1.37 ppm); [c)]The molecular weights were calculated using ^{1}H NMR by integrating the methoxy peak of mPEO at 3.37 ppm and the peak for the repeating units of εCL and γBL; [d)]Determined by SEC using tetrahydrofuran as the eluent; [e)]Critical aggregation concentrations were determined at room temperature in PBS; [f)]When DACCA-labeled copolymers were used, the content of DACCA was determined by UV–vis spectroscopy.

Nanoparticles were successfully prepared from the copolymers using the nanoprecipitation technique, resulting in final sample concentrations of 1 mg·mL^{-1}. Fresh nanoformulations were prepared for each characterization, following a previously published procedure.[4]

The images obtained using the cryogenic transmission electron microscopy (cryo-TEM) and graphs using data from dynamic light scattering (DLS) and flow field-flow fractionation (A4F) are shown in **Figure 10**. The critical aggregation concentrations (CAC) were measured and the values for each sample are listed in **Table 3**. All the CACs are on the order of micrograms per milliliter, so it confirms that aggregates form at the concentration that was used.

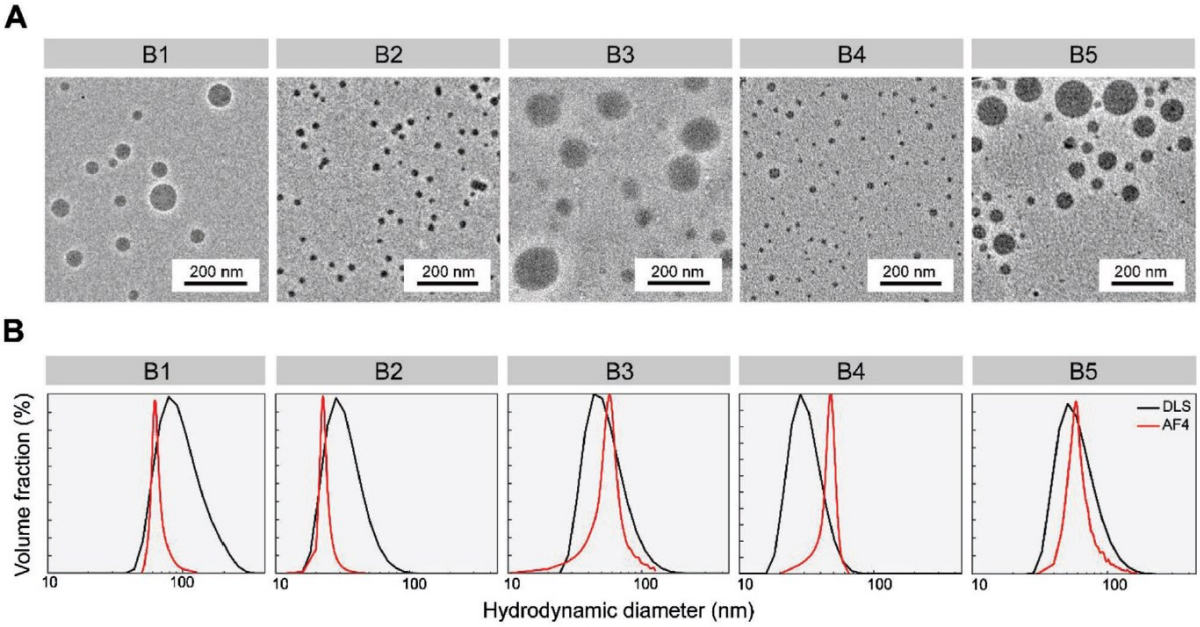

Figure 10: Nanoparticles' characterization. **A)** Images taken by cryo-TEM. **B)** NPs' size distribution determined by dynamic light scattering (black) and asymmetric flow field-flow fractionation (red).[77]

Detailed characteristics of the prepared NPs are summarized in **Table 4**. When comparing the Z-average hydrodynamic diameter obtained by DLS with the Z-average diameter of gyration obtained by SLS and AF4, the values show a close correlation. These coherent data are supported by the weight-average molar mass values measured by SLS and A4F.

Table 4: Characteristics of prepared nanoparticles.[77]

Sample	D_H^{DLS} a) [nm]	PDI a) DLS	D_G^{SLS} b) [nm]	M_W^{SLS} b) [kDa]	ρ^{SLS} c) [g mL^{-1}]	D_G^{AF4} b) [nm]	M_W^{AF4} b) [kDa]	ρ^{AF4} c) [g mL^{-1}]	N_{agg}^{AF4} d)
B1	109	0.113	91	14 900	0.029	77	101 400	0.324	9050
B2	41	0.188	40	5800	0.134	26	8160	0.690	710
B3	71	0.166	120	13 800	0.012	85	24 700	0.060	1110
B4	36	0.109	48	1000	0.013	47	4180	0.060	420
B5	71	0.111	170	38 100	0.011	103	66 700	0.091	2510

a)The Z-average of the hydrodynamic diameter D_H and polydispersity index PDI; b)The molecular weight M_W and the Z-average of the diameter of gyration D_G; c)The apparent structural density was calculated from the equation $\rho = 6M_w/\pi N_A D^3$ considering a spherical shape ($D = 1.29 \cdot D_G$); d)The aggregation number is the quotient of the M_W of the particles (AF4) and the M_W of the polymer (SEC).

The combined results from DLS, AF4, and cryo-TEM provided insights into the structure of the nanoparticles (NPs). While mPEO-b-PCL-based assemblies are often described as micelles, our AF4 data indicate that each NP contains approximately 400–9000 polymer chains, significantly more than the 10–100 chains typical of micelles. The apparent structural density (ρ) of the particles, calculated using the molecular weight and assuming a spherical model, showed that mPEO-b-(PCL-co-P4HB) NPs were about three times less dense than mPEO-b-PCL NPs. This lower

density suggests that the presence of 4HB results in a less dense, less hydrophobic core, potentially affecting cargo encapsulation.

The comprehensive characterization of NPs enabled us to fine-tune nanoparticle parameters, allowing for more precise design tailored to specific application requirements in the future.

3.1.3. Biological tests of the NPs

The following biological tests were conducted to ensure the safe, effective, and predictable use of prepared NPs in biomedical applications. The biocompatibility of these NPs was described in previously published literature[78] and the cytotoxicity of prepared NPs is discussed below.

First, the cytotoxicity of the prepared formulations (B1-B5) was assessed using MTT assay after a 24-hour incubation with J774A.1 macrophage cells. The results, as shown in **Figure 11**, indicate that cell viability was only minimally affected by the nanoformulations. The copolymer cytotoxicity was found to be nearly negligible at clinically relevant concentrations, demonstrating that the introduction of P4HB within the copolymeric matrix did not compromise the biocompatibility of the nanoparticles with J774A.1 cells. This suggests that the synthesized NPs are safe for biomedical applications.

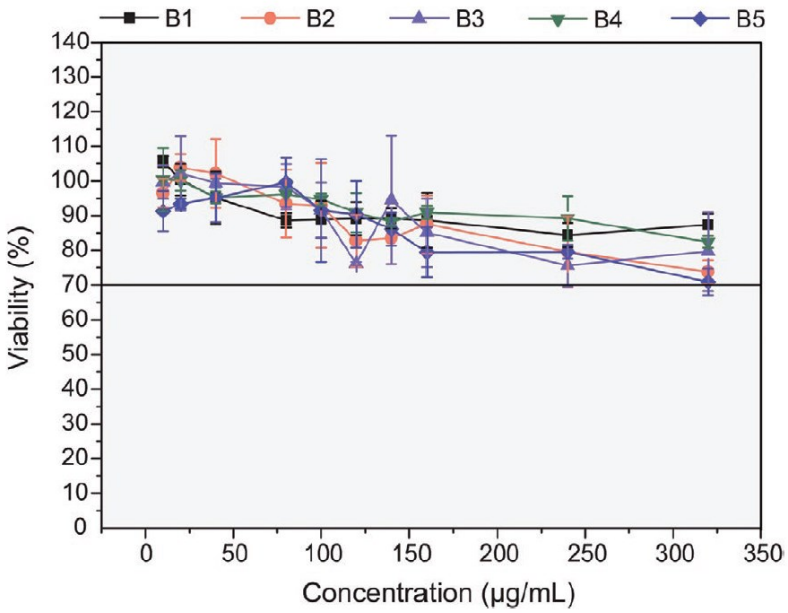

Figure 11: Viability of J774A.1 cells detected by MTT assay. Murine monocyte-macrophages were incubated with varying NP concentrations for 24 hours, and viability was analyzed by measuring metabolically produced formazan. The horizontal line indicates the threshold for distinguishing between non-cytotoxic (above) and cytotoxic (below) viability levels.[77]

Secondly, the hemolysis assay was performed to evaluate the blood compatibility and potential membrane toxicity of the prepared NPs. Red blood cells were mixed with various NP dilutions and incubated, after which hemolysis was measured. The results showed that hemoglobin release was below 2% for all dilutions, classifying the NPs as nonhemolytic and confirming their safety for biomedical applications.

Additionally, the degradation of the NPs was studied to describe the influence of butyrolactone units in the hydrophobic block in the copolymer chain. The enzymatic degradation of the NPs in vitro under the influence of lipase is described in the following paragraph 3.1.3.1. In this study, degradation was also monitored intracellularly in macrophage-like cells; information on cellular uptake and intracellular degradation is provided in paragraph 3.1.3.2.

3.1.3.1. Degradation of NPs *in vitro*

The *in vitro* enzymatic degradation tests were conducted in an NMR test tube by adding a sample of the NP formulation in PBS and mixing it with lipase from *Pseudomonas* sp., resulting in a final copolymer concentration of 0.98 $mg \cdot mL^{-1}$ and a lipase concentration of 0.06 $U \cdot mL^{-1}$. By observing the reduction of certain signals in the ^{1}H NMR spectra over time of samples B1 and B3 after the lipase addition, the degradation rate was determined. The results indicated that degradation occurs more rapidly when only caprolactone units are present in the hydrophobic block (B1). Conversely, when additionally butyrolactone units are present in the hydrophobic block of the copolymer (B3), the NPs tend to degrade slower, providing space for on-demand tailoring of the degradability rate of the nanoparticles.

The degradation of the samples was confirmed by SEC by measuring the average molar mass over time. Detailed information is available in the attached article (**Appendix 2**).

3.1.3.2. Intracellular degradation

For confocal laser scanning microscopy (CLSM), the NP samples required fluorescent labeling. Thus, 7-(diethylamino)coumarin-3-carbonyl azide (DACCA) was reacted with samples B1-B5. The content of DACCA in each sample is detailed in **Table 3**.

The cellular uptake of these labeled NPs by macrophage-like J774A.1 cells was examined. Internalization of the DACCA-labeled NPs was observed within 40 minutes (**Figure 12**), revealing differences in intracellular distribution patterns. Markers for low pH compartments indicated that all NP samples targeted acidic organelles (**Figure 13**), as confirmed by Pearson correlation

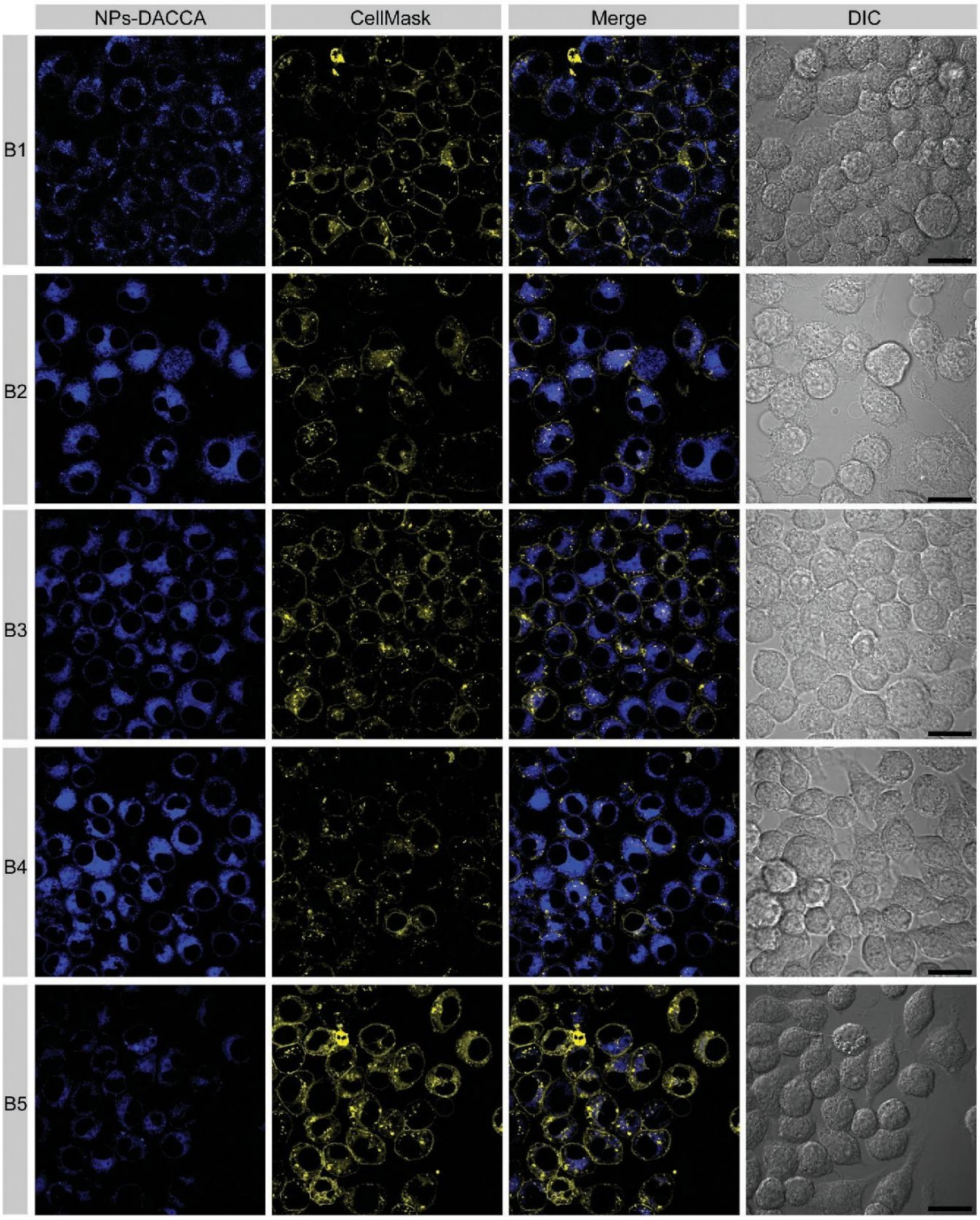

Figure 12: Study of DACCA-labeled NP uptake by J774A.1 cells. Fluorescence and differential interference contrast (DIC) images of J774A.1 cells were captured 40 minutes post-addition of DACCA-labeled NPs (2.8 nmol mL^{-1}, blue fluorescence). The CellMask Deep Red signal, related to the plasma membrane, is displayed in yellow. Scale bars represent 20 µm.[77]

coefficient (PCC) values. These findings suggest that such systems are usable as a logical strategy for effectively killing intracellular microbes.[79]

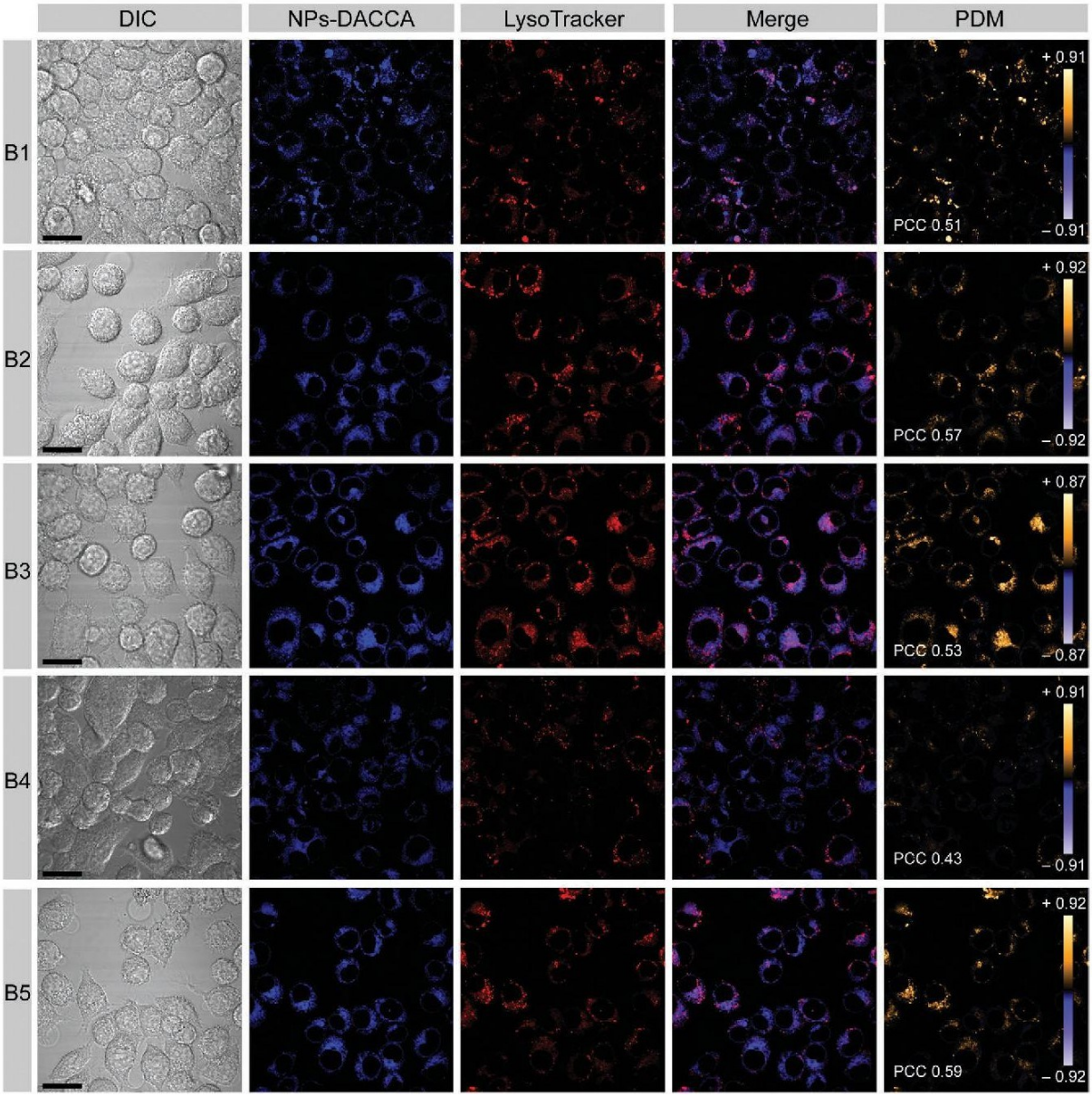

Figure 13: Localization of DACCA-labeled NPs in J774A.1 Cells. CLSM images of J774A.1 macrophages 40 minutes post-treatment with DACCA-labeled NPs (2.8 nmol mL^{-1}) and LysoTracker. Colocalization analysis was performed using Product of the Differences from the Mean (PDM) images and Pearson Correlation Coefficient (PCC) values. PDM images are pseudocolored, with pixel colors representing PDM values: orange for colocalized pixels and blue for segregated areas. Scale bars: 20 µm. Differential Interference Contrast (DIC) is indicated.[77]

To investigate the cellular internalization kinetics of DACCA-labeled nanoparticles (NPs) in J774A.1 macrophage-like cells, NPs at a concentration of 2 nmol mL^{-1} were incubated with cell monolayers for varying times. Flow cytometry analysis (**Figure 14A**) showed that NP uptake increased with incubation time, reaching peak fluorescence intensity after 60-100 minutes. Internalization half-time (τ1/2) was calculated from the data using a curve-fitting approach, revealing a notable difference among samples. For instance, the P4HB-free mPEO45-b-PCL81 (B1) had a significantly longer τ1/2 (~54 min) compared to mPEO45-b-(PCL55-co-P4HB19) (B3), which had a τ1/2 of ~9.5 min, despite having similar hydrophilic/hydrophobic ratios and molecular weights. This variation suggests that P4HB introduction affects NP uptake, potentially due to changes in crystallinity or NP size.

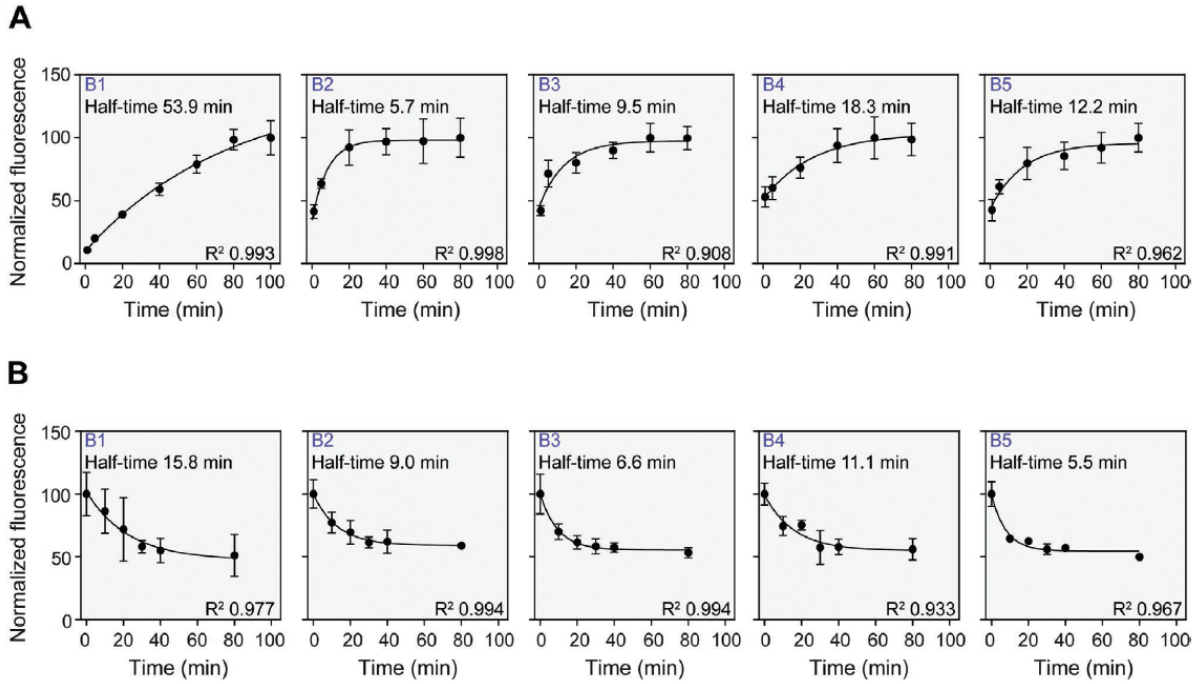

Figure 14: Investigation of DACCA-labeled nanoparticle (NP) behavior. **A)** Time course of cell-associated fluorescence following the addition of 2 nmol mL−1 DACCA-labeled NPs. The fluorescence data were normalized to the maximum values achieved (plateau values). **B)** Time course of NP degradation after incubating monolayers with 2 nmol mL−1 DACCA-labeled NPs for 60 minutes. The graph shows both half-time and R-squared values.[77]

Further, after reaching peak fluorescence, a decline was observed, likely due to enzymatic degradation of the DACCA matrix as DACCA is more fluorescent in a hydrophobic environment of intact nanoparticle cores than if released free in aqueous solution by degradation of the nanoparticles. To assess degradation kinetics, NPs were incubated for 60 minutes, then washed

and analyzed over time using flow cytometry (**Figure 14B**). The degradation rate constant was derived from a single exponential decay model, showing that all NP formulations exhibited similar degradation patterns, indicating colocalization with acidic organelles. Notably, B1 displayed the slowest degradation rate ($\tau 1/2 \approx 16$ min), suggesting that P4HB can modulate NP degradation. Flow cytometry results aligned with the hypothesis that lysosomal localization correlates with faster degradation, contrasting with 1H NMR studies conducted in PBS. This discrepancy underscores the importance of studying NP behavior in more complex environments, such as in the presence of serum and cellular proteins. The enzymatic degradation of mPEO-b-(PCL-co-P4HB) copolymers to biocompatible products like mPEO, 6-hydroxyhexanoic acid, and 4-hydroxybutyric acid suggests favorable in vivo behavior, as these products are metabolized and eliminated efficiently by the body.

3.2. Nanocrystals

The skin serves crucial roles including protection and moisture control but is vulnerable to infections due to injuries and chronic conditions. Rising antibiotic resistance necessitates innovative solutions for such infections. Nanotechnology presents promising alternatives, particularly in the form of nanostructures like antibacterial nanobeads, which offer enhanced antimicrobial activity and reduced side effects. Recent studies have explored various nanostructures, including metal and lipid nanoparticles, for treating bacterial and fungal skin infections. This work focuses on chloroxine, an 8-hydroxyquinoline derivative with known antimicrobial properties but limited by low water solubility. In the work attached in **Appendix 3**, chloroxine nanoparticles (CXNPs), a stable colloidal formulation stabilized with a biocompatible surfactant, are characterized for the aforementioned purposes. Their nanostructural properties were measured using dynamic light scattering (DLS), and their antimicrobial effectiveness and skin safety *in vivo* are evaluated.

3.2.1. Chloroxine nanoparticles preparation and characterization

The CXNPs were prepared by rapid pouring an ethanol solution of chloroxine into an aqueous phase (either water or a surfactant solution), followed by the removal of ethanol under reduced pressure and slightly elevated temperature. Three surfactants—Tween 80 (TW80), Brij 92 (BR92), and Brij 700 (BR700)—were tested for stabilizing CXNPs in the aqueous phase. These surfactants were used in four different concentrations, all below their critical micelle concentration (CMC). The specific concentrations of surfactants used were chosen based on their CMC values. For each surfactant, the samples were prepared at varying concentrations, specifically 20%, 40%, 60%, and 80% of their respective CMC values. This approach ensured a comprehensive evaluation of the surfactant's stabilizing capabilities at different levels relative to their CMC.

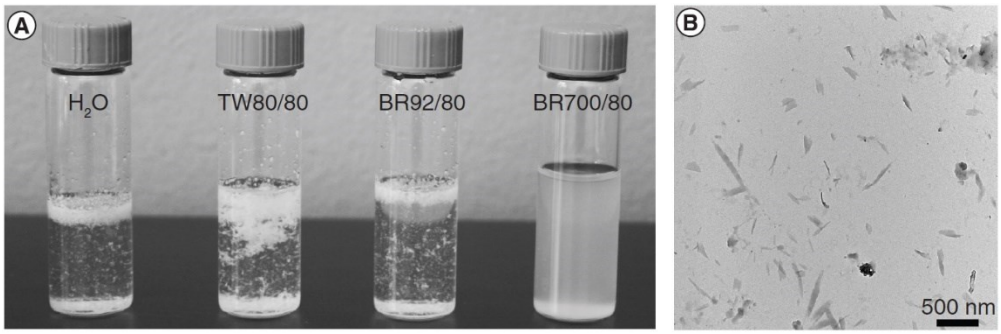

Figure 15: Chloroxine precipitation in different aqueous media. **A)** Macroscopic structure of chloroxine precipitations in vials (pure water, Tween80, Brij72 and Brij 700) **B)** TEM image of the CXNPs stabilized by Brij700.[80]

As shown in **Figure 15A** and supported by the data in **Table 5**, the nanoformulation that avoided significant precipitation was prepared using Brij700 as a surfactant. Additionally, the TEM image in **Figure 15B** shows the nanostructured elongated crystals of this formulation. This formulation was analyzed by DLS, which measured the hydrodynamic diameter of the stabilized nanocrystals to be 580 nm with broad size distribution. The zero zeta potential indicates steric stabilization and decrease of the surface charge. The sizes and zeta potentials of the CXNPs of all samples are provided for comparison in **Table 5**.

Table 5: Physicochemical properties of CXNPs as measured.[80]

Sample	D_H ± SD (nm)	ζ ± SD (mV)	note
TW80/20	1035 ± 26	-23,0 ± 0,6	GP
TW80/40	1026 ± 70	-29,4 ± 1,1	GP
TW80/60	903 ± 34	-29,8 ± 0,8	GP
TW80/80	548 ± 55	-30,8 ± 1,0	GP
BR92/20	1153 ± 55	-34,6 ± 0,8	GP
BR92/40	496 ± 51	-35,3 ± 5,7	GP
BR92/60	517 ± 87	-35,1 ± 4,1	GP
BR92/80	324 ± 73	-35,0 ± 1,2	GP
BR700/20	831 ± 17	-18,9 ± 0,6	HF
BR700/40	654 ± 13	0,0 ± 0,1	HF
BR700/60	608 ± 5	0,0 ± 0,1	HF
BR700/80	580 ± 26	0,0 ± 0,1	HF

The number after the slash in the sample name indicates the surfactant concentration as a percentage of its CMC. Samples TW80 and BR92 were analyzed after centrifugation (1500 r.p.m., 10 min). D_H: Hydrodynamic diameter; GP: Gross precipitation, centrifugation necessary; HF: Homogeneous formulation, no centrifugation needed; SD: Standard deviation.

3.2.2. Cytotoxicity of CXNPs

The effect of nanoformulation labelled as BR700/80 on cell viability was evaluated using a resazurin assay. Two human skin cell lines, A431 epithelial cells and HaCaT keratinocytes, were tested to assess dermal cytocompatibility *in vitro*. The cytotoxicity of these CXNPs was found to be incubation time-dependent. For the A431 cell line, IC50 values of 31.6 ± 6.9 µg/ml after 48 hours and 5.9 ± 1.3 µg/ml after 72 hours were determined, with no IC50 reached at 24 hours. In

HaCaT cells, IC50 values of 26.0 ± 10 µg/ml at 24 hours, 12.0 ± 2.1 µg/ml at 48 hours, and 6.1 ± 2.3 µg/ml at 72 hours were observed.

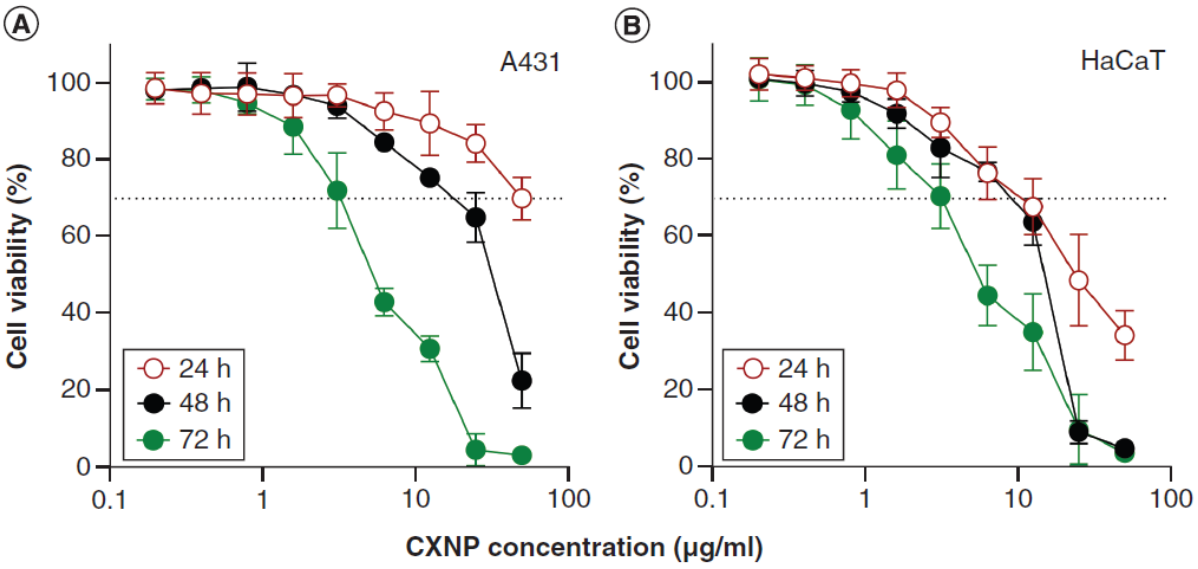

Figure 16: Cytotoxicity of CXNPs – sample BR700/80. **A)** Human skin epithelial A431 cells and **B)** HaCaT human skin keratinocytes were exposed to different concentrations of CXNPs for 24, 48, and 72 hours. Cytotoxicity was measured using the resazurin assay. Horizontal dotted line represents cell viability threshold, with values above the line indicating non-cytotoxicity and values below indicating cytotoxicity. Results are shown as mean values ± standard deviation.[80]

3.2.3. Antimicrobial properties of CXNPs

The CXNPs – sample BR700/80 exhibited significant antimicrobial activity against a variety of medically important pathogens listed in **Table 6** in a broth microdilution assay. For Gram-positive bacteria, the MIC (minimum inhibitory concentration) was approximately 5 µg/ml across all strains, with MBC (minimum bactericidal concentration) values showing bactericidal effects for *C. pseudodiphtheriticum* (5–6 µg/mL) and *S. epidermidis* (1,5 µg/mL), while *S. aureus* and *S. pyogenes* did not reveal bactericidal effects within the tested concentration range. Among Gram-negative bacteria, the MIC varied, with *C. sakazakii*, *P. aeruginosa*, and *S. marcescens* showing higher resistance (MIC ~12 µg/mL), and *B. bronchiseptica* and *S. flexneri* being more sensitive (MIC ~4 µg/mL). However, most Gram-negative species did not exhibit bactericidal effects (MBC >50 µg/ml), aligning with chloroxine's microbiostatic properties. Notably, *M. catarrhalis* showed the best activity with both MIC and MBC ≤0,05 µg/mL. The formulation also demonstrated

antifungal potency, with MIC values of 0,2; 12,5; and 1,6 µg/mL for *Can. albicans*, *M. furfur*, and *M. pachydermatis*, respectively, and fungicidal MBC values ranging from 0,2 to 12,5 µg/mL.

Table 6: Antimicrobial properties of CXNPs – sample BR700/80.[80]

Group	Strain	Designation	Note	MIC (µg/mL)	MBC (µg/mL)
G+ bacteria	*Corynebacterium pseudodiphtheriticum*	CCM 2821	TS	5	5-6
	Staphylococcus aureus subsp. *aureus*	CCM 4223		5	> 50
	Staphylococcus aureus subsp. *aureus*	ATCC 33591	Methicillin-resistant	5	> 50
	Staphylococcus epidermidis	CCM 2124	TS	5	12,5
	Streptococcus pyogenes	CCM 7418		5-6	> 50
G– bacteria	*Acinetobacter baumannii*	CCM 2355	TS	5-6	25
	Bordetella bronchiseptica	CCM 6082	TS	4	> 50
	Cronobacter sakazakii	CCM 1902		11-12,5	> 50
	Enterobacter cloacae	CCM 8574	TS	8-9	> 50
	Escherichia coli	CCM 3954		5-6	> 50
	Klebsiella oxytoca	CCM 1901		5-6	6,25-12,5
	Klebsiella pneumoniae subsp. *pneumoniae*	CCM 7798	TS	6-7	> 50
	Moraxella catarrhalis	CCM 2828		≤ 0,5	≤ 0,5
	Pseudomonas aeruginosa	CCM 1960	TS	12,5	> 50
	Serratia marcescens	CCM 303	TS	12	> 50
	Shigella flexneri	CCM 4422		3-4	> 50
Fungi	*Candida albicans*	CCM 8261		0,2	0,2-0,4
	Candida albicans	CCM 8215		0,2	0,4
	Malassezia furfur	DSM 6170		12,5	12,5
	Malassezia pachydermatis	DSM 6172		1,6	1,6-3

The maximum concentration tested was 50 µg/mL

ATCC: American type Culture Collection, CCM: Czech collection of microorganisms, DSM: Deutsche Sammlung von Mikroorganismen und Zellkulturen (German Collection of Microorganisms and Cell Cultures), MIC: minimum inhibitory concentration, MBC: minimum bactericidal concentration, TS: type strain

3.2.4. Skin irritation tests of CXNPs *in vivo*

A dermatological test was conducted to assess whether CXNPs – sample BR700/80 cause skin irritation in mice. BALB/c mice were divided into four groups, each containing five mice, and had their dorsal fur shaved. Different treatments were administered to each group: a sham control with Brij 700 solution, and CXNPs at concentrations of 25 µg/ml and 50 µg/ml. The formulations were applied daily for seven days using a nonwoven polyethylene cloth fixed to the mice's backs.

Daily inspections measured transepidermal water loss (TEWL), skin pH, and erythema (redness). After seven days, the mice were sacrificed for histopathological examination of the skin.

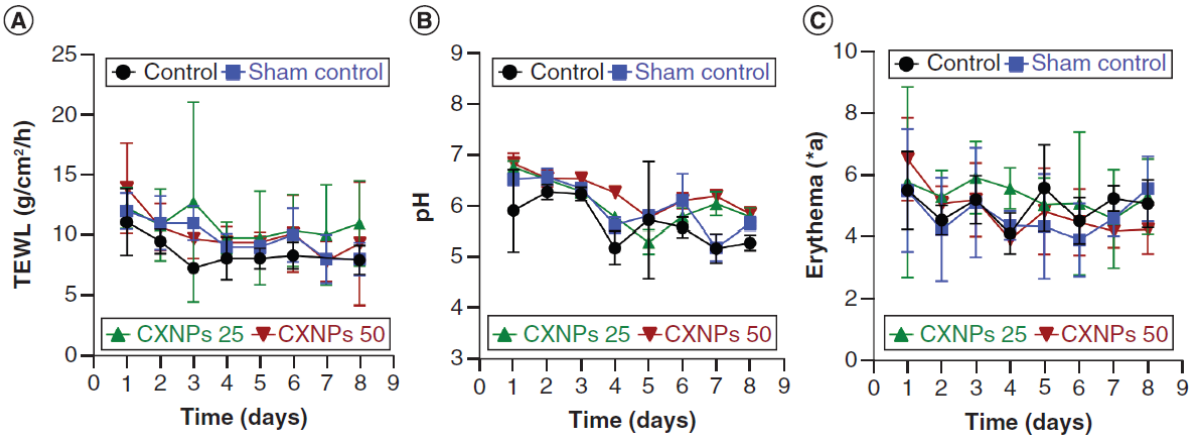

Figure 17: The *in vivo* skin tolerance of CXNPs – sample BR700/80 was evaluated over a 7-day treatment period on mouse skin. Measurements included **A)** transepidermal water loss (TEWL), **B)** skin pH, and **C)** skin erythema (redness, a*). The data are presented as mean values with standard deviations.[80]

As evident from the graphs in **Figure 17**, no significant changes were observed in TEWL, pH, or erythema, indicating no skin irritation. Moreover, histopathological analysis confirmed no pathological changes in the skin tissues, demonstrating that CXNPs are well-tolerated and non-toxic, making them suitable for topical applications.

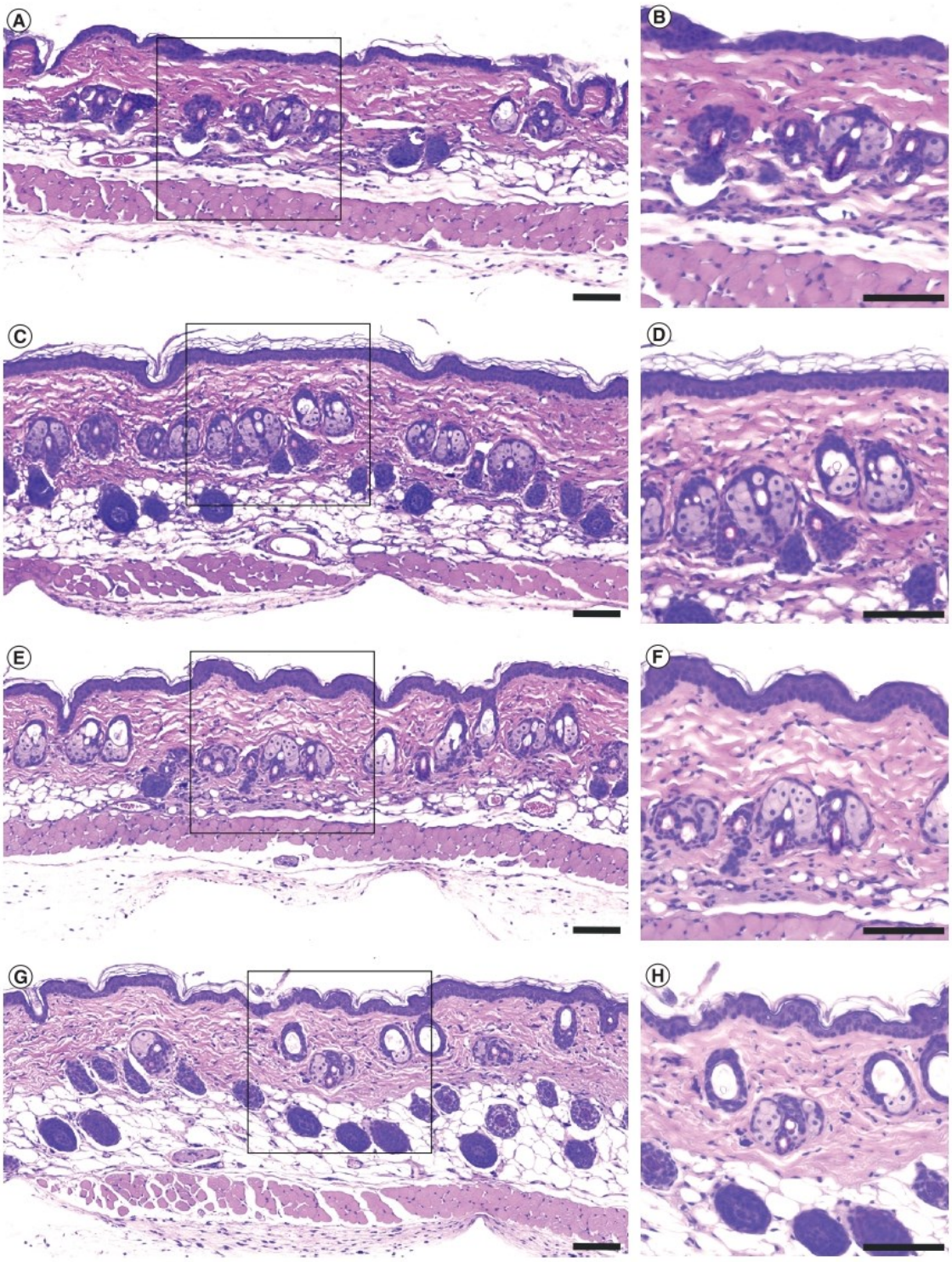

Figure 18: *In vivo* skin tolerance test of CXNPs – sample BR700/80 was evaluated through histopathological examination (hematoxylin & eosin staining) of mouse dorsal skin 7 days post-treatment. **A, B)** skin sections from untreated mice, **C, D)** skin from mice exposed to the Brij 700 solution, **E, F)** skin from mice treated with CXNPs at 25 µg/mL, and **G, H)** skin from mice treated with 50 µg/mL. Scale bars represent 100 µm.[80]

3.3. Polymer layer sensors

In a significant number of joint replacements, serious infections can occur, often necessitating reoperation. One potential method to prevent this complication is the early detection of infection before the formation of hard-to-eliminate mature bacterial biofilm. To facilitate this, a modified metallized polyporphyrin sensing layer was designed to enable *in situ* sensing of reactive oxygen species (ROS), which are strongly associated with inflammations and infections.

A robust potentiometric sensor for detecting reactive ROS was developed and applied as a thin layer on smart implant surfaces to enable early inflammation detection. The sensor consists of a polythiophene-based conductive polymer layer with an embedded porphyrin-metal complex for ROS detection. The sensing layer was cast on a glassy carbon support and coated with poly(2-methyl-2-oxazoline) to prevent interference from proteins and other biomolecules. Four different metal cations (Fe^{2+}, Co^{2+}, Cu^{2+}, and Mn^{2+}) were incorporated into the porphyrin core. The sensor with Fe^{2+} ions was specifically tested for its response to ROS, demonstrating high sensitivity and the ability to distinguish between hydrogen peroxide and hypochlorite, while maintaining functionality in the presence of potential biological interferences.

For more detailed information, the entire article on this research can be found in **Appendix 4**.

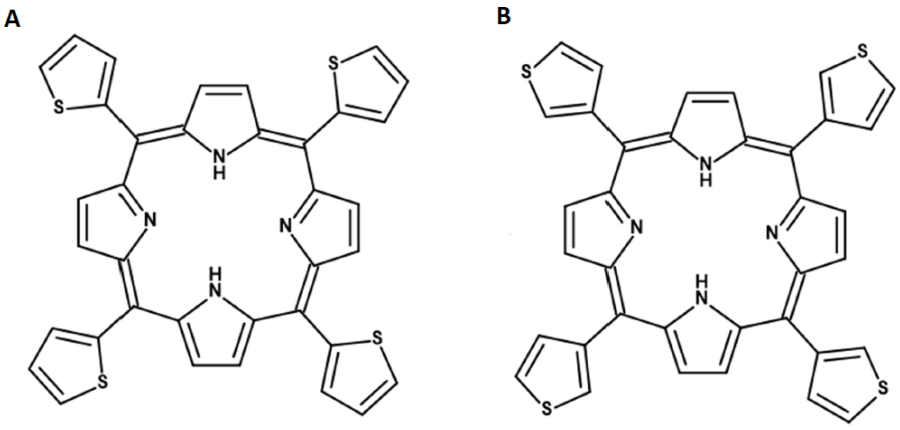

Figure 19: Structures of synthetized porphyrin derivatives **A)** 2TTP (5,10,15,20-tetra(thien-2-yl)porphyrin) and **B)** 3TTP (5,10,15,20-tetra(thien-3-yl)porphyrin).[81]

3.3.1. Preparation and characterization of porphyrin-based sensing layer

Two different derivatives of porphyrin, 2TTP and 3TTP (5,10,15,20-tetra(thien-2-yl)porphyrin and 5,10,15,20-tetra(thien-3-yl)porphyrin, both structures shown in **Figure 19**), were synthesized by reacting either 2-thiophenecarboxaldehyde or 3-thiophenecarboxaldehyde with

pyrrole in propionic acid under reflux and elevated temperature. In both syntheses, the products as brown crystals were yielded. The crystals were purified and then used for electropolymerization to form the sensing layer. As evident from the structures seen in **Figure 19**, the molecule of 2TTP is a tetra-functional monomer whereas 3TTP is an octa-functional monomer.

The electropolymerization of 2TTP or 3TTP was conducted in a solution of formic acid with the addition of 1-methylimidazole in CH_2Cl_2 in a three-electrode cell using a potentiostat under an inert nitrogen atmosphere. The fluorine-doped tin oxide (FTO) and glassy carbon (GC) electrodes were used as the working electrodes, a platinum sheet as the counter electrode, and silver wire as a reference electrode. During the polymerization, the potential was cycled 50 times between -1 and 1,85 V at a scan rate of 50 $mV \cdot s^{-1}$. For 2TTP, successful deposition occurred on both FTO and GC supports, while 3TTP only deposited on GC. After electropolymerization, the electrodes were washed with chloroform to remove any unreacted monomers or by-products. The cleaned electrodes were then stored in a desiccator to keep them dry and prevent contamination.

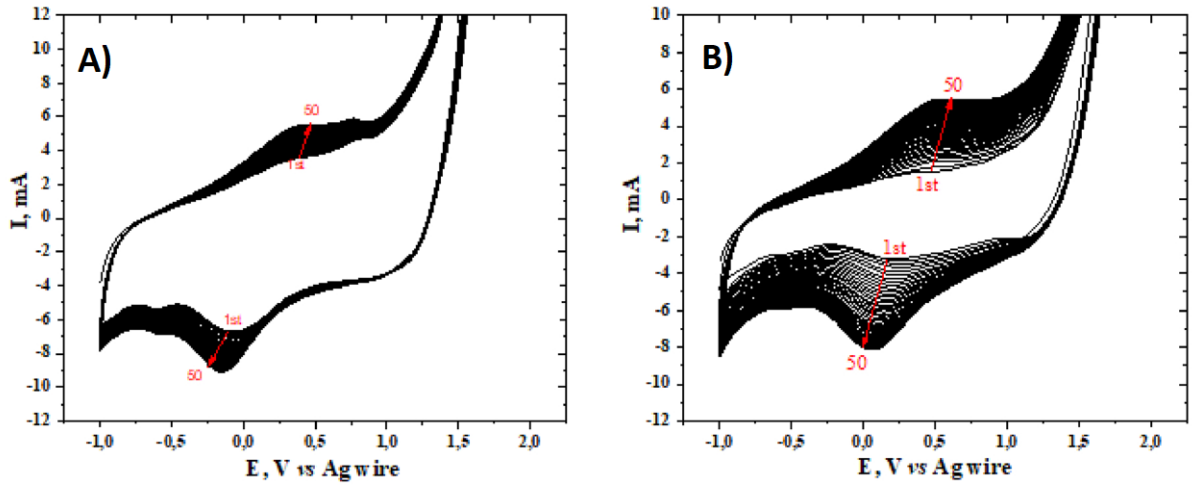

Figure 20: Electropolymerization curves of **A)** 2TTP on FTO and **B)** 3TTP on GC in CH_2Cl_2 containing 5 M formic acid.[81]

The characterization of the deposited polymer porphyrin-based layers involved several analytical techniques to assess their structural, morphological, and electrochemical properties. The cyclic voltammetry curves of 2TTP (**Figure 20A**) showed two oxidation and two reduction peaks, indicating the formation of dimers at specific positions. Whereas the cyclic voltametric curves of 3TTP (**Figure 20B**) showed one oxidation and one reduction peak, with a higher oxidation potential compared to 2TTP.

The surface morphology of the deposited films was examined by scanning electron microscopy (SEM). The film created by electropolymerization of 3TTP (poly-3TTP, **Figure 21B**) exhibited a rough surface, while the film created by electropolymerization of 2TTP (poly-2TTP, **Figure 21A**)

showed a smoother and more compact layer. Comparisons with bare FTO and GC electrodes highlighted the increased surface area provided by the poly-3TTP film.

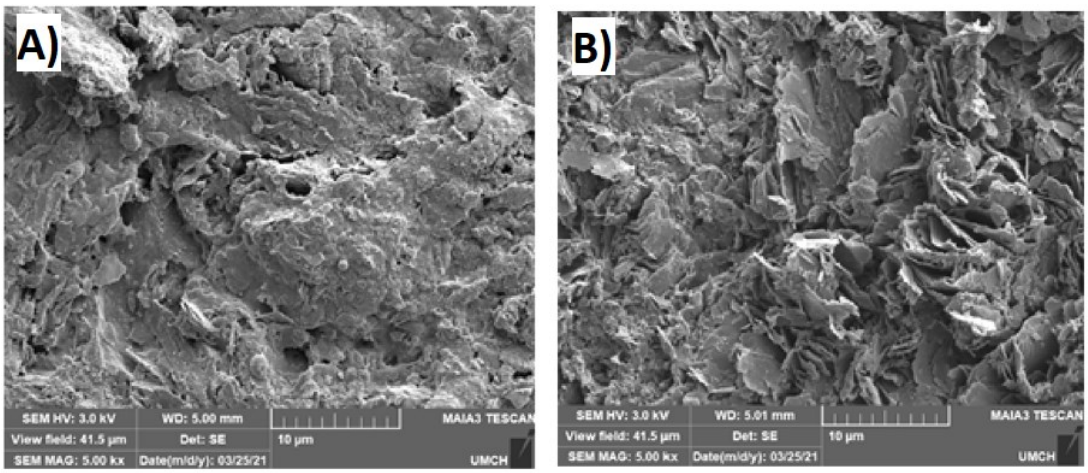

Figure 21: SEM images of **A)** poly-2TTP on FTO and **B)** poly-3TTP on GC, both at 10 000x magnification.[81]

Raman spectra were measured for both monomers (2TTP and 3TTP) and their corresponding polymer films (poly-2TTP and poly-3TTP). The polymer films exhibited broadening and an increase in the intensity of Raman signals compared to the monomers. This broadening is indicative of polymer formation, as it reflects changes in the molecular structure and the creation of larger polymeric chains (conductive polymeric films).

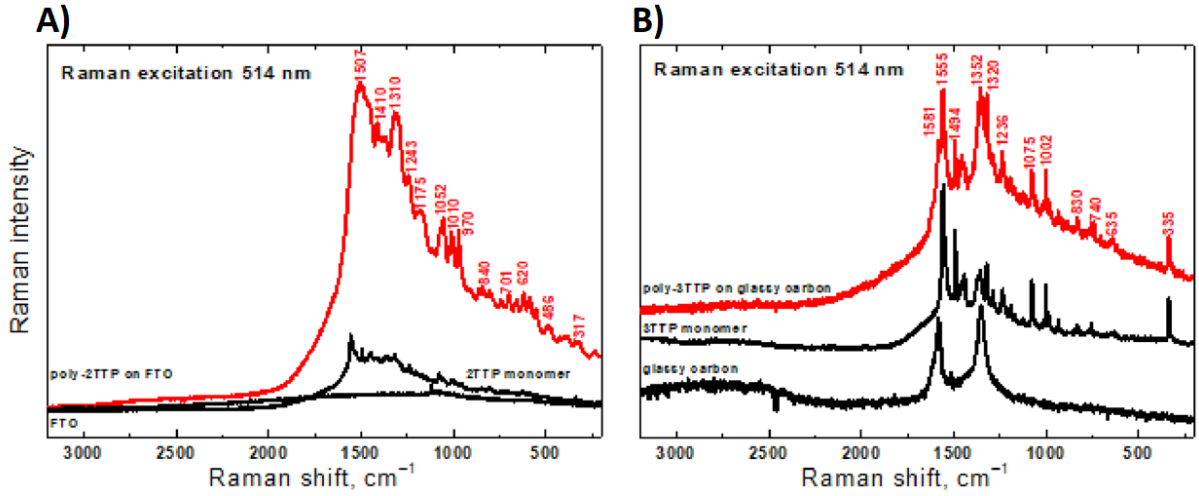

Figure 22: Raman spectra (excitation laser at 514 nm) of **A)** poly-2TTP on FTO (red line), with the spectra of the 2TTP monomer and FTO (both in black lines) added for comparison, and **B)** poly-3TTP on GC (red line), with the spectra of the 3TTP monomer and GC (both in black lines) added for comparison.[81]

The X-ray Diffraction (XRD) was utilized to analyze the crystalline structure and orientation of the porphyrin rings in the polymer films poly-2TTP and poly-3TTP. A significant peak was observed at 2Θ = 16°, corresponding to the distance between the porphyrin rings. The presence of this peak indicates a regular, periodic arrangement of the porphyrin molecules within the polymer films. The intensity of the peak at 2Θ = 16° was higher for poly-2TTP than for poly-3TTP. This higher intensity suggests that the porphyrin rings in poly-2TTP are more organized and better aligned compared to those in poly-3TTP. The better organization in poly-2TTP is likely due to its tetra-functional nature, offering four positions for electropolymerization. In contrast, poly-3TTP, being octa-functional with eight positions for electropolymerization, has a more complex structure, leading to less orderly arrangement of the porphyrin rings.

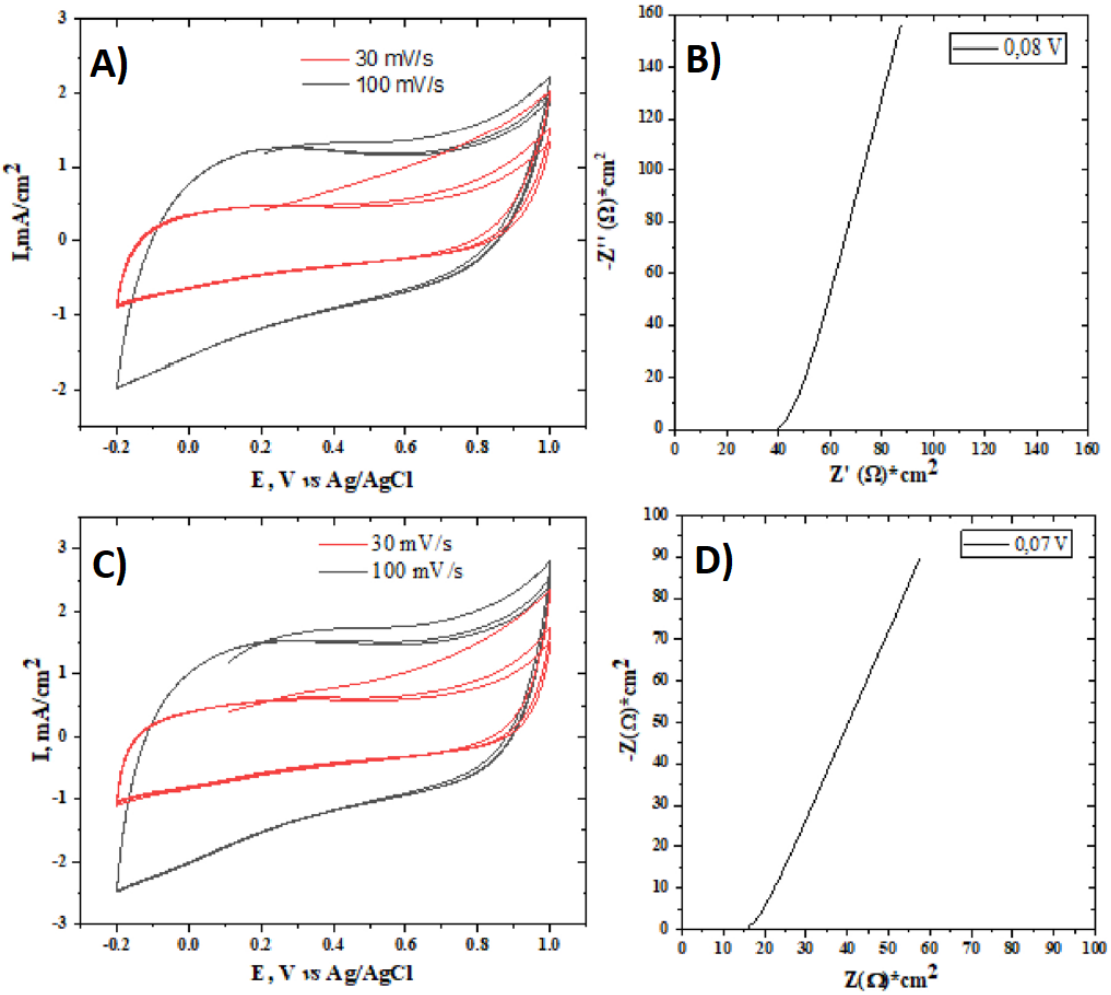

Figure 23: Characteristics of poly-3TTP on GC measured in PBS buffer by **A)** electrochemical cyclic voltammetry and **B)** EIS at 0,08 V vs. Ag/AgCl (corresponding to V_{oc}); characteristics of poly-2TTP on FTO measured in PBS buffer by **C)** electrochemical cyclic voltammetry and **D)** EIS at 0,07 V vs. Ag/AgCl (correspond to V_{oc}).[81]

The electrochemical characterization of poly-3TTP and poly-2TTP films, as presented in **Figure 23**, reveals significant differences in their suitability for sensing applications. Cyclic voltammetry data shows that both polymers exhibit distinct redox activity, confirming their electroactive nature (**Figure 23A** and **C**). However, the electrochemical impedance spectroscopy (EIS) results highlight a key difference: poly-3TTP displays a capacitive impedance character, indicative of a large interface area and efficient charge storage (**Figure 23B**), which are advantageous for sensing applications. In contrast, poly-2TTP exhibits a diffusion-controlled impedance behavior (**Figure 23D**), suggesting a different molecular arrangement that may be less ideal for sensor performance. These findings suggest that poly-3TTP, with its favorable capacitive properties, is better suited for further development as a sensing layer.

3.3.2. Porphyrin-based sensing layer doped with metals

The doping of the poly-3TTP on GC with metals was carried out through a specific procedure to incorporate metal cations into the porphyrin core, which is present in the poly-3TTP film.

3.3.2.1. Doping of 3-TTP film by metals

Four different metal cations (Fe^{2+}, Co^{2+}, Cu^{2+}, and Mn^{2+}) were selected for incorporation into the poly-3TTP film. 1 M aqueous solutions of $FeCl_2$, $CoCl_2$, $CuCl_2$, and $MnCl_2$ were prepared. The samples of poly-3TTP films on GC were immersed in the corresponding metal solution for 24 hours. During this time, the metal cations were chelated into the porphyrin core of the poly-3TTP film, effectively doping the polymer with the metal ions. After the doping process, the films were identified as poly-3TTP-Cu, poly-3TTP-Fe, poly-3TTP-Co, and poly-3TTP-Mn, depending on the metal incorporated.

The presence of the metal ions within the porphyrin structure was confirmed using high-resolution X-ray photoelectron spectroscopy (XPS). The XPS spectra showed changes, such as the appearance of new peaks corresponding to the metal-chelated nitrogen in the porphyrin ring, confirming successful metal doping.

3.3.2.2. Electrochemical sensitivity

In this experiment, the sensitivity of poly-3TTP-Cu and poly-3TTP-Fe layers to H_2O_2 was assessed using a potentiometric approach. The polymer films deposited on GC electrodes which served as the working electrodes in a three-electrode cell setup, with a platinum sheet as the counter electrode and a silver/silver chloride (Ag/AgCl) electrode as the reference. The electrodes were immersed in a PBS solution at pH 7. H_2O_2 was sequentially added to the solution at concentrations ranging from 50 nM to 10 μM. The potential difference between the working and reference electrodes was measured for each concentration after allowing the potential to stabilize.

The results shown in **Figure 24** highlight that the poly-3TTP-Fe sensing layer is more sensitive to hydrogen peroxide than the poly-3TTP-Cu layer. This enhanced sensitivity is reflected in the steeper slope and broader linear range, making poly-3TTP-Fe a more promising candidate for detecting biologically relevant concentrations of H_2O_2. Specifically, the poly-3TTP-Cu layer exhibits a linear response from 50 nM to 1 µM with a slope of 13.54 ± 0.5 mV/decade (R^2 = 0.9939), while the poly-3TTP-Fe layer demonstrates a linear response from 50 nM to 10 µM with a slope of 31.75 ± 0.5 mV/decade (R^2 = 0.9995).

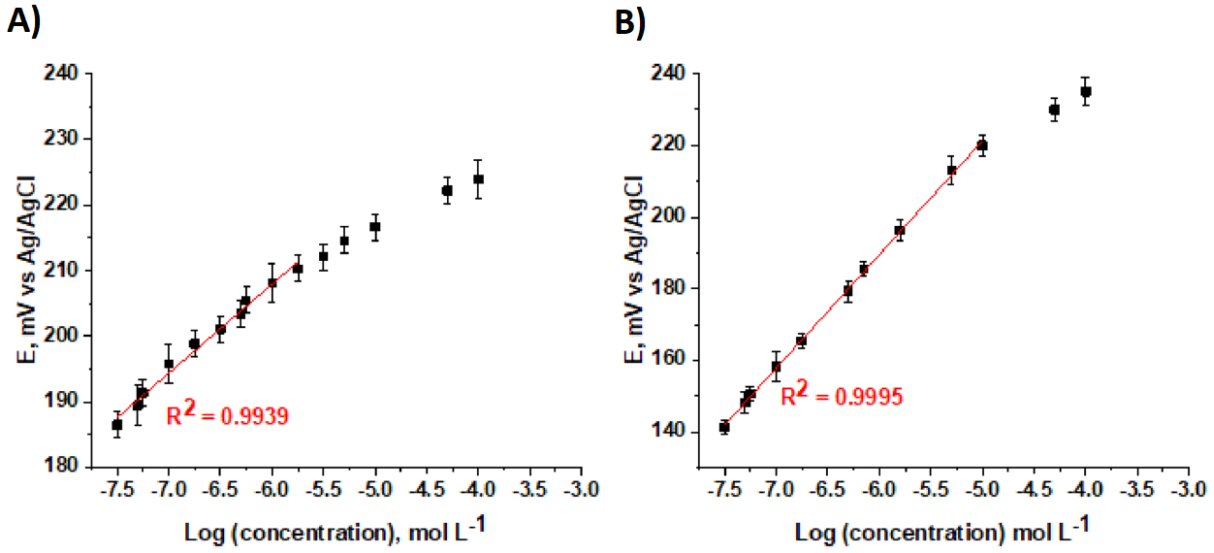

Figure 24: Potentiometric response curves of **A)** poly-3TTP-Cu and **B)** poly-3TTP-Fe sensing layers for detecting varying concentrations of H_2O_2 in PBS at pH 7.[81]

3.3.3. Nonbiofouling of the porphyrin-based sensing layer

To ensure the sensor's effectiveness in detecting reactive oxygen species (ROS) in healthy tissue, it is crucial to prevent biofouling. Biofouling, which involves the accumulation of proteins and other biological materials on the sensor surface, can interfere with its functionality and accuracy. By incorporating a nonbiofouling layer, such as poly(2-methyl-oxazoline) (PMeOx), the sensor surface is protected from these unwanted interactions, allowing for precise and reliable ROS detection in healthy tissue environments.

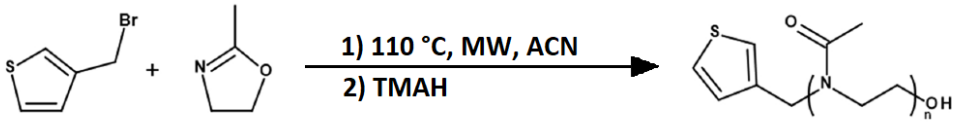

Figure 25: Polymerization scheme of α-thiophene poly(2-methyl-2-oxazoline).[81]

For that purpose, microwave-assisted cationic ring-opening polymerization was conducted as schematically shown in **Figure 25**. The monomer, 2-methyl-2-oxazoline, was dissolved in acetonitrile, with 3-(bromomethyl)thiophene serving as the initiator. The monomer-to-initiator ratio (n_M/n_I) was adjusted to synthesize three types of α-thiophene poly(2-methyl-2-oxazoline) with different molar masses (1, 2 and 5 kDa). The characteristics of these polymers are listed in the accompanying table.

Table 7: The polymerization parameters and characteristics of synthetized PMeOx.[81]

	n_M/n_I	M_n *a)* (kDa)	M_n *b)* (kDa)	$Đ$ *b)*
P1	11,7	1,5	1,5	1,15
P2	23,5	3,0	2,4	1,24
P3	58,7	4,6	5,4	1,24

a) Number average of molar mass *Mn* determined by ^{1}H NMR *b)* Number average of molar mass *Mn* and dispersity *Đ* were determined by SEC.

These three purified samples of *α*-thiophene poly(2-methyl-2-oxazoline) with different chain lengths were applied on the sensor's surface, utilizing the thiophene rings' ability to facilitate attachment. However, XPS analysis revealed that only the highest molecular weight PMeOx (P3) successfully formed a detectable layer on poly-3TTP-Fe.

The final sensor, named poly-3TTP-Fe/PMeOx, was tested in the presence of bovine serum albumin and catalase to evaluate its nonbiofouling properties and sensitivity to H_2O_2.

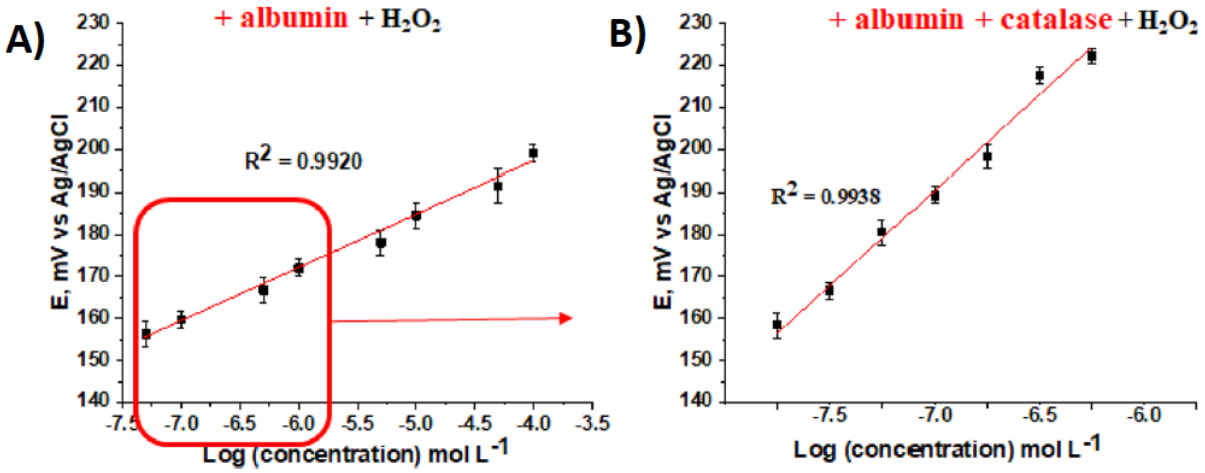

Figure 26: Potentiometric detection of H_2O_2 in PBS (pH = 7) using the poly-3TTP-Fe/PMeOx sensing layer **A)** in the presence of albumin and **B)** in the presence of albumin with catalase.[81]

The results in **Figure 26A** showed that the sensor exhibited a linear response to H_2O_2 in the presence of albumin, with a detection range from 50 nM to 100 µM and a slope of 12.84 mV/decade. In the presence of catalase, the sensor's sensitivity improved, with a slope of 44.4 mV/decade (shown in **Figure 26B**), possibly due to redox interactions between catalase and the sensing layer.

The electrochemical impedance spectra of the poly-3TTP-Fe/PMeOx sensor before and after exposure to bovine serum albumin were compared in **Figure 27**. The similarity in the spectra indicated that the PMeOx layer effectively prevented albumin from attaching to the sensor surface, preserving its electrochemical properties.

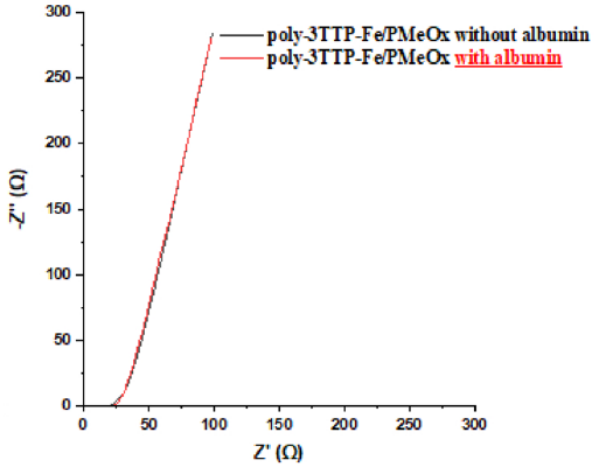

Figure 27: Electrochemical impedance spectra of poly-3TTP-Fe/PMeOx before (black line) and after (red line) measurement in albumin.[81]

The poly-3TTP-Fe/PMeOx sensor demonstrated stability for at least one month, showing consistent performance upon repeated testing. These findings suggest that the poly-3TTP-Fe/PMeOx sensor is a promising candidate for accurate and sensitive online monitoring of H_2O_2 in complex biological environments.

3.3.4. Selectivity of poly-3TTP-Fe/PMeOx sensor

To confirm that the poly-3TTP-Fe/PMeOx sensor is selectively responsive to H_2O_2, potentiometric detection of hypochlorite (ClO^-), another marker of bacterial infection, was tested at relevant concentrations. The results in **Figure 28** showed no significant response of the sensor to ClO^- in the concentration range of 50 nM to 10 µM, except at the highest concentrations, which are not biologically relevant. This indicates that the poly-3TTP-Fe/PMeOx sensing layer is specifically suited for H_2O_2 detection and that the presence of ClO^- will not interfere with its performance.

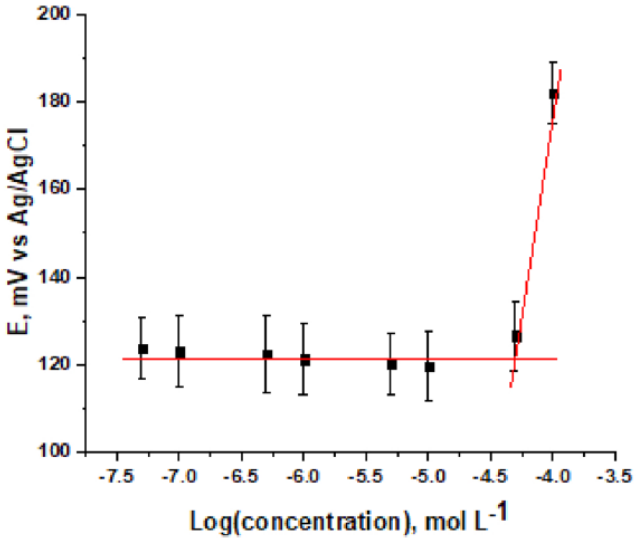

Figure 28: Potentiometric detection of ClO^- ions in PBS (pH = 7) using the poly-3TTP-Fe/PMeOx.[81]

4. Summary and future perspectives

This thesis successfully addresses the critical challenges posed by infectious diseases and inflammation, particularly in the context of increasing antibiotic resistance, by developing innovative supramolecular biocompatible polymer nanosystems for bioapplications. The research demonstrates the versatility and efficacy of polymer-based approaches in three distinct areas. The first area involves the preparation and characterization of block copolymers, specifically poly(ethylene oxide)-*b*-poly(*ε*-caprolactone) modified with *γ*-butyrolactone, resulting in materials with tailored enzymatic degradation profiles that were effectively utilized to construct a delivery system for the antibiotic rifampicin, demonstrating potential for enhancing the treatment of bacterial infections. The second area explores the stabilization of antimicrobial nanoparticles, where the self-assembled chloroxine with polymeric non-ionic surfactants led to the successful formation of stable nanocrystalline particles, significantly improving the solubility and stability of chloroxine, and highlighting the potential of polymer-stabilized nanoparticles in overcoming challenges associated with poorly soluble antimicrobial drugs. The third area focuses on the development of a polymer layer-type potentiometric sensor for detecting inflammation-related reactive oxygen species (ROS), which represents a significant advancement in diagnostic technology, as the sensor, based on porphyrin cores with embedded metal ions and protected by poly(2-methyl-2-oxazoline), demonstrated high sensitivity and specificity, enabling the early detection of inflammation and infection. Overall, this thesis contributes valuable knowledge to the field of polymer science and its application in medicine, offering promising strategies for the treatment and detection of infectious diseases and inflammation, and underscoring the potential of polymer-based systems to address some of the most pressing biomedical challenges of our time.

Future advancements in antibacterial delivery systems will most plausibly focus on further tailoring drug release profiles and nanoparticle degradation rates, as well as enhancing the selective targeting of nanoparticles to pathogens or pathogen-infected cells, including intracellular pathogens. Strategies involving external stimuli-triggered release of active pharmaceutical ingredients, along with the incorporation of microfluidics for precise control over nanoparticle size, are expected to play a significant role. The use of stimuli-responsive polymersomes is also anticipated. While the covalent attachment of drugs to polymer carriers offers greater control over release rates, it introduces a new prodrug chemical entity, which could present challenges in the regulatory approval process.

The integration of fundamentally new antibacterial agents into polymer nanoparticles and polymer-stabilized nanocrystals is urgently needed, as the portfolio of clinically used antibacterial agents has stagnated. The lack of novel active pharmaceutical ingredients might lead to severe increasing microbial resistance against current therapeutic strategies.

In the realm of inflammation and infection sensors, future developments will likely enable the detection of additional infection-specific analytes, such as free calcium, defensins, and lipopolysaccharides. This progress could lead to the creation of a miniaturized implantable chip equipped with multiple electrodes for the simultaneous in situ detection of several analytes—a "chemical tongue" selective for infection. Such a device could be incorporated into medical implants, such as hip or knee replacements, to facilitate early detection of infections.

5. References

1. Ratner, B. D.; Zhang, G., 1.1.2 - A History of Biomaterials. In *Biomaterials Science (Fourth Edition)*, Wagner, W. R.; Sakiyama-Elbert, S. E.; Zhang, G.; Yaszemski, M. J., Eds. Academic Press: 2020; pp 21-34.
2. Crubzy, E.; Murail, P.; Girard, L.; Bernadou, J.-P., False teeth of the Roman world. *Nature* **1998,** *391* (6662), 29-29.
3. "Hermann Staudinger". https://www.britannica.com/biography/Hermann-Staudinger (accessed 30 July 2021).
4. Trousil, J.; Syrová, Z.; Dal, N.-J. K.; Rak, D.; Konefał, R.; Pavlova, E.; Matějková, J.; Cmarko, D.; Kubíčková, P.; Pavliš, O.; Urbánek, T.; Sedlák, M.; Fenaroli, F.; Raška, I.; Štěpánek, P.; Hrubý, M., Rifampicin Nanoformulation Enhances Treatment of Tuberculosis in Zebrafish. *Biomacromolecules* **2019,** *20* (4), 1798-1815.
5. Jäger, E.; Sincari, V.; Albuquerque, L. J. C.; Jäger, A.; Humajova, J.; Kucka, J.; Pankrac, J.; Paral, P.; Heizer, T.; Janouskova, O.; Konefał, R.; Pavlova, E.; Sedlacek, O.; Giacomelli, F. C.; Pouckova, P.; Sefc, L.; Stepanek, P.; Hruby, M., Reactive Oxygen Species (ROS)-Responsive Polymersomes with Site-Specific Chemotherapeutic Delivery into Tumors via Spacer Design Chemistry. *Biomacromolecules* **2020,** *21* (4), 1437-1449.
6. Kaberov, L. I.; Kaberova, Z.; Murmiliuk, A.; Trousil, J.; Sedláček, O.; Konefal, R.; Zhigunov, A.; Pavlova, E.; Vít, M.; Jirák, D.; Hoogenboom, R.; Filippov, S. K., Fluorine-Containing Block and Gradient Copoly(2-oxazoline)s Based on 2-(3,3,3-Trifluoropropyl)-2-oxazoline: A Quest for the Optimal Self-Assembled Structure for 19F Imaging. *Biomacromolecules* **2021,** *22* (7), 2963-2975.
7. Jirak, D.; Galisova, A.; Kolouchova, K.; Babuka, D.; Hruby, M., Fluorine polymer probes for magnetic resonance imaging: quo vadis? *Magnetic Resonance Materials in Physics, Biology and Medicine* **2019,** *32* (1), 173-185.
8. *Biomaterials Market Size, Share & Trends Analysis Report*; Grand View Research: 2020.
9. Kadajji, V. G.; Betageri, G. V., Water Soluble Polymers for Pharmaceutical Applications. *Polymers* **2011,** *3* (4), 1972-2009.
10. D'souza, A. A.; Shegokar, R., Polyethylene glycol (PEG): a versatile polymer for pharmaceutical applications. *Expert Opinion on Drug Delivery* **2016,** *13* (9), 1257-1275.
11. Winger, M.; de Vries, A. H.; van Gunsteren, W. F., Force-field dependence of the conformational properties of α,ω-dimethoxypolyethylene glycol. *Molecular Physics* **2009,** *107* (13), 1313-1321.
12. Bailey, F. E.; Koleske, J. V., Polyoxyalkylenes. In *Ullmann's Encyclopedia of Industrial Chemistry*.
13. Webster, R.; Elliott, V.; Park, B. K.; Walker, D.; Hankin, M.; Taupin, P., PEG and PEG conjugates toxicity: towards an understanding of the toxicity of PEG and its relevance to PEGylated biologicals. In *PEGylated Protein Drugs: Basic Science and Clinical Applications*, Veronese, F. M., Ed. Birkhäuser Basel: Basel, 2009; pp 127-146.
14. Shiraishi, K.; Yokoyama, M., Toxicity and immunogenicity concerns related to PEGylated-micelle carrier systems: a review. *Science and Technology of Advanced Materials* **2019,** *20* (1), 324-336.
15. de la Rosa, V. R., Poly(2-oxazoline)s as materials for biomedical applications. *Journal of Materials Science: Materials in Medicine* **2014,** *25* (5), 1211-1225.

16. Bludau, H.; Czapar, A. E.; Pitek, A. S.; Shukla, S.; Jordan, R.; Steinmetz, N. F., POxylation as an alternative stealth coating for biomedical applications. *European Polymer Journal* **2017,** *88*, 679-688.

17. Kosakowska, K. A.; Dimitrov, P.; Panambur, G.; Grayson, S. M., MALDI-TOF MS investigation of the unconventional termination of living polyoxazoline with ammonia. *Journal of Polymer Science Part A: Polymer Chemistry* **2017,** *55* (8), 1303-1312.

18. Chytil, P.; Kostka, L.; Etrych, T., HPMA Copolymer-Based Nanomedicines in Controlled Drug Delivery. *Journal of Personalized Medicine* **2021,** *11* (2).

19. Tucker, B. S.; Sumerlin, B. S., Poly(N-(2-hydroxypropyl) methacrylamide)-based nanotherapeutics. *Polymer Chemistry* **2014,** *5* (5), 1566-1572.

20. Scales, C. W.; Vasilieva, Y. A.; Convertine, A. J.; Lowe, A. B.; McCormick, C. L., Direct, Controlled Synthesis of the Nonimmunogenic, Hydrophilic Polymer, Poly(N-(2-hydroxypropyl)methacrylamide) via RAFT in Aqueous Media. *Biomacromolecules* **2005,** *6* (4), 1846-1850.

21. Franco, P.; De Marco, I., The Use of Poly(N-vinyl pyrrolidone) in the Delivery of Drugs: A Review. *Polymers (Basel)* **2020,** *12* (5).

22. Committee, J. F., *British National Formulary (BNF) 69*. Pharmaceutical Press: 2015.

23. Vert, M., Aliphatic Polyesters: Great Degradable Polymers That Cannot Do Everything. *Biomacromolecules* **2005,** *6* (2), 538-546.

24. Albertsson, A.-C.; Varma, I. K., Recent Developments in Ring Opening Polymerization of Lactones for Biomedical Applications. *Biomacromolecules* **2003,** *4* (6), 1466-1486.

25. Labet, M.; Thielemans, W., Synthesis of polycaprolactone: a review. *Chemical Society Reviews* **2009,** *38* (12), 3484-3504.

26. Woodard, L. N.; Grunlan, M. A., Hydrolytic Degradation and Erosion of Polyester Biomaterials. *ACS Macro Letters Journal* **2018,** *7* (8), 976-982.

27. Martin, D. P.; Williams, S. F., Medical applications of poly-4-hydroxybutyrate: a strong flexible absorbable biomaterial. *Biochemical Engineering Journal* **2003,** *16* (2), 97-105.

28. Ulery, B. D.; Nair, L. S.; Laurencin, C. T., Biomedical Applications of Biodegradable Polymers. *Journal of Polymer Science B Polymer Physics* **2011,** *49* (12), 832-864.

29. Marten, E.; Müller, R.-J.; Deckwer, W.-D., Studies on the enzymatic hydrolysis of polyesters I. Low molecular mass model esters and aliphatic polyesters. *Polymer Degradation and Stability* **2003,** *80* (3), 485-501.

30. Piluso, S.; Lendlein, A.; Neffe, A. T., Enzymatic action as switch of bulk to surface degradation of clicked gelatin-based networks. *Polymers for Advanced Technologies* **2017,** *28* (10), 1318-1324.

31. J. Prokeš, J. S., M. Omastová, Polyaniline and Polypyrrole - Two Representatives of Conducting Polymers *Chemické listy* **2001,** *95* (8), 484-492.

32. Naarmann, H., Synthesis of new conductive polymers. *Synthetic Metals* **1987,** *17* (1), 223-228.

33. Naarmann, H.; Theophilou, N., New process for the production of metal-like, stable polyacetylene. *Synthetic Metals* **1987,** *22* (1), 1-8.

34. Gueye, M. N.; Carella, A.; Faure-Vincent, J.; Demadrille, R.; Simonato, J.-P., Progress in understanding structure and transport properties of PEDOT-based materials: A critical review. *Progress in Materials Science* **2020,** *108*, 100616.

35. MacDiarmid, A. G.; Mammone, R. J.; Kaner, R. B.; Porter, L.; Pethig, R.; Heeger, A. J.; Rosseinsky, D. R.; Gillespie, R. J.; Day, P., The concept of 'doping' of conducting polymers: the role of reduction potentials. *Philosophical Transactions of the Royal Society of London. Series A, Mathematical and Physical Sciences* **1985,** *314* (1528), 3-15.

36. Voss, D., Cheap and cheerful circuits. *Nature* **2000,** *407* (6803), 442-444.

37. Loukotová, L.; Švec, P.; Groborz, O.; Heizer, T.; Beneš, H.; Raabová, H.; Bělinová, T.; Herynek, V.; Hrubý, M., Direct Comparison of Analogous Amphiphilic Gradient and Block Polyoxazolines. *Macromolecules* **2021,** *54* (17), 8182-8194.

38. Urbánek, T.; Jäger, E.; Jäger, A.; Hrubý, M., Selectively Biodegradable Polyesters: Nature-Inspired Construction Materials for Future Biomedical Applications. *Polymers* **2019,** *11* (6), 1061.

39. Gregory, A.; Stenzel, M. H., Complex polymer architectures via RAFT polymerization: From fundamental process to extending the scope using click chemistry and nature's building blocks. *Progress in Polymer Science* **2012,** *37* (1), 38-105.

40. Mieras, H. J. M. A., Solution and bulk flow properties of linear and branched styrene–butadiene rubbers. *Journal of Polymer Science: Polymer Symposia* **1973,** *42* (2), 987-1000.

41. Hussain, M.; Naqvi, R. A.; Abbas, N.; Khan, S. M.; Nawaz, S.; Hussain, A.; Zahra, N.; Khalid, M. W., Ultra-High-Molecular-Weight-Polyethylene (UHMWPE) as a Promising Polymer Material for Biomedical Applications: A Concise Review. *Polymers* **2020,** *12* (2), 323.

42. Mai, Y.; Eisenberg, A., Self-assembly of block copolymers. *Chemical Society Reviews* **2012,** *41* (18), 5969-5985.

43. Kim, J.; Mok, M. M.; Sandoval, R. W.; Woo, D. J.; Torkelson, J. M., Uniquely Broad Glass Transition Temperatures of Gradient Copolymers Relative to Random and Block Copolymers Containing Repulsive Comonomers. *Macromolecules* **2006,** *39* (18), 6152-6160.

44. Wong, C. L. H.; Kim, J.; Roth, C. B.; Torkelson, J. M., Comparison of Critical Micelle Concentrations of Gradient Copolymer and Block Copolymer in Homopolymer: Novel Characterization by Intrinsic Fluorescence. *Macromolecules* **2007,** *40* (16), 5631-5633.

45. Lombardo, D.; Kiselev, M. A.; Magazù, S.; Calandra, P., Amphiphiles Self-Assembly: Basic Concepts and Future Perspectives of Supramolecular Approaches. *Advances in Condensed Matter Physics* **2015,** *2015*, 151683.

46. Schalley, C. A., Introduction. In *Analytical Methods in Supramolecular Chemistry*, 2006; pp 1-16.

47. Levin, A.; Hakala, T. A.; Schnaider, L.; Bernardes, G. J. L.; Gazit, E.; Knowles, T. P. J., Biomimetic peptide self-assembly for functional materials. *Nature Reviews Chemistry* **2020,** *4* (11), 615-634.

48. Lombardo, D.; Kiselev, M. A.; Magazù, S.; Calandra, P., Amphiphiles Self-Assembly: Basic Concepts and Future Perspectives of Supramolecular Approaches. *Advances in Condensed Matter Physics* **2015,** *2015* (1), 151683.

49. Schärtl, W., *Light Scattering from Polymer Solutions and Nanoparticle Dispersions* Springer-Verlag: Berlin Heidelberg, 2007.

50. Brožek, J., *Fyzikální chemie polymerů*. VŠCHT Praha: 2019.

51. Bhattacharjee, S., DLS and zeta potential – What they are and what they are not? *Journal of Controlled Release* **2016,** *235*, 337-351.

52. Lindner, P.; Zemb, T. In *Neutrons, X-rays and light : scattering methods applied to soft condensed matter*, 2002.

53. Pennycook, S. J., Fulfilling Feynman's dream: "Make the electron microscope 100 times better"—Are we there yet? *MRS Bulletin* **2015,** *40* (1), 71-78.

54. Abbe, E., Beiträge zur Theorie des Mikroskops und der mikroskopischen Wahrnehmung. *Archiv für Mikroskopische Anatomie* **1873,** *9* (1), 413-468.

55. Dillard, R. S.; Hampton, C. M.; Strauss, J. D.; Ke, Z.; Altomara, D.; Guerrero-Ferreira, R. C.; Kiss, G.; Wright, E. R., Biological Applications at the Cutting Edge of Cryo-Electron Microscopy. *Microscopy and Microanalysis* **2018,** *24* (4), 406-419.

56. Osada, Y.; Rossi, D. E. D., *Polymer Sensors and Actuators*. 1 ed.; Springer-Verlag: Berlin Heidelberg, 2000.

57. Cichosz, S.; Masek, A.; Zaborski, M., Polymer-based sensors: A review. *Polymer Testing* **2018,** *67*, 342-348.

58. Medlock, K.; Harmer, H.; Worsley, G.; Horgan, A.; Pritchard, J., pH-sensitive holograms for continuous monitoring in plasma. *Analytical and Bioanalytical Chemistry* **2007,** *389* (5), 1533-1539.

59. Lavine, B. K.; Kaval, N.; Oxenford, L.; Kim, M.; Dahal, K. S.; Perera, N.; Seitz, R.; Moulton, J. T.; Bunce, R. A., Synthesis and Characterization of N-Isopropylacrylamide Microspheres as pH Sensors. *Sensors* **2021,** *21* (19), 6493.

60. Bird, R. E.; Lemmel, S. A.; Yu, X.; Zhou, Q. A., Bioorthogonal Chemistry and Its Applications. *Bioconjugate Chemistry* **2021,** *32* (12), 2457-2479.

61. Jackson, C.; Anderson, A.; Alexandrov, K., The present and the future of protein biosensor engineering. *Current Opinion in Structural Biology* **2022,** *75*, 102424.

62. Faridbod, F.; Norouzi, P.; Dinarvand, R.; Ganjali, M. R., Developments in the Field of Conducting and Non-conducting Polymer Based Potentiometric Membrane Sensors for Ions Over the Past Decade. *Sensors (Basel)* **2008,** *8* (4), 2331-2412.

63. Goldberg, H. D.; Brown, R. B.; Liu, D. P.; Meyerhoff, M. E., Screen printing: a technology for the batch fabrication of integrated chemical-sensor arrays. *Sensors and Actuators B: Chemical* **1994,** *21* (3), 171-183.

64. Lindfors, T.; Ivaska, A., Calcium-selective electrode based on polyaniline functionalized with bis[4-(1,1,3,3-tetramethylbutyl)phenyl]phosphate. *Analytica Chimica Acta* **2001,** *437* (2), 171-182.

65. Özbek, O.; Isildak, Ö.; Berkel, C., The use of porphyrins in potentiometric sensors as ionophores. *Journal of Inclusion Phenomena and Macrocyclic Chemistry* **2020,** *98* (1), 1-9.

66. Vlascici, D.; Fagadar-Cosma, E.; Pica, E. M.; Cosma, V.; Bizerea, O.; Mihailescu, G.; Olenic, L., Free Base Porphyrins as Ionophores for Heavy Metal Sensors. *Sensors (Basel)* **2008,** *8* (8), 4995-5004.

67. Cheng, L.; Meng, Q.-H.; Lilienthal, A. J.; Qi, P.-F., Development of compact electronic noses: a review. *Measurement Science and Technology* **2021,** *32* (6), 062002.

68. Syrový, T.; Kuberský, P.; Sapurina, I.; Pretl, S.; Bober, P.; Syrová, L.; Hamáček, A.; Stejskal, J., Gravure-printed ammonia sensor based on organic polyaniline colloids. *Sensors and Actuators B: Chemical* **2016,** *225*, 510-516.

69. Kuberský, P.; Syrový, T.; Hamáček, A.; Nešpůrek, S.; Stejskal, J., Printed Flexible Gas Sensors based on Organic Materials. *Procedia Engineering* **2015,** *120*, 614-617.

70. Jiang, H.; Lin, Q.; Yu, Z.; Wang, C.; Zhang, R., Nanotechnologies for Reactive Oxygen Species"Turn-On" Detection. *Frontiers in Bioengineering and Biotechnology* **2021,** *9*.

71. Murphy, M. P.; Bayir, H.; Belousov, V.; Chang, C. J.; Davies, K. J. A.; Davies, M. J.; Dick, T. P.; Finkel, T.; Forman, H. J.; Janssen-Heininger, Y.; Gems, D.; Kagan, V. E.; Kalyanaraman, B.; Larsson, N.-G.; Milne, G. L.; Nyström, T.; Poulsen, H. E.; Radi, R.; Van Remmen, H.; Schumacker, P. T.; Thornalley, P. J.; Toyokuni, S.; Winterbourn, C. C.; Yin, H.; Halliwell, B., Guidelines for measuring reactive oxygen species and oxidative damage in cells and in vivo. *Nature Metabolism* **2022,** *4* (6), 651-662.

72. Duanghathaipornsuk, S.; Farrell, E. J.; Alba-Rubio, A. C.; Zelenay, P.; Kim, D. S., Detection Technologies for Reactive Oxygen Species: Fluorescence and Electrochemical Methods and Their Applications. *Biosensors (Basel)* **2021,** *11* (2).

73. Karjalainen, E.; Aseyev, V.; Tenhu, H., Upper or lower critical solution temperature, or both? Studies on cationic copolymers of N-isopropylacrylamide. *Polymer Chemistry* **2015,** *6* (16), 3074-3082.

74. Ward, M. A.; Georgiou, T. K., Thermoresponsive Polymers for Biomedical Applications. *Polymers* **2011,** *3* (3), 1215-1242.

75. Groborz, O.; Kolouchová, K.; Pankrác, J.; Keša, P.; Kadlec, J.; Krunclová, T.; Pierzynová, A.; Šrámek, J.; Hovořáková, M.; Dalecká, L.; Pavlíková, Z.; Matouš, P.; Páral, P.; Loukotová, L.; Švec, P.; Beneš, H.; Štěpánek, L.; Dunlop, D.; Melo, C. V.; Šefc, L.; Slanina, T.; Beneš, J.; Van Vlierberghe, S.; Hoogenboom, R.; Hrubý, M., Pharmacokinetics of Intramuscularly Administered Thermoresponsive Polymers. *Advanced Healthcare Materials* **2022,** *11* (22), 2201344.

76. Hu, J.; Liu, S., Responsive Polymers for Detection and Sensing Applications: Current Status and Future Developments. *Macromolecules* **2010,** *43* (20), 8315-8330.

77. Urbánek, T.; Trousil, J.; Rak, D.; Gunár, K.; Konefał, R.; Šlouf, M.; Sedlák, M.; Šebestová Janoušková, O.; Hrubý, M., γ-Butyrolactone Copolymerization with the Well-Documented Polymer Drug Carrier Poly(ethylene oxide)-block-poly(ε-caprolactone) to Fine-Tune Its Biorelevant Properties. *Macromolecular Bioscience* **2020,** *20* (5), e1900408.

78. Moore, T.; Adhikari, R.; Gunatillake, P., Chemosynthesis of bioresorbable poly(gamma-butyrolactone) by ring-opening polymerisation: a review. *Biomaterials* **2005,** *26* (18), 3771-82.

79. Tiwari, R.; Gupta, R. P.; Singh, V. K.; Kumar, A.; Rajneesh; Madhukar, P.; Sundar, S.; Gautam, V.; Kumar, R., Nanotechnology-Based Strategies in Parasitic Disease Management: From Prevention to Diagnosis and Treatment. *ACS Omega* **2023,** *8* (45), 42014-42027.

80. Trousil, J.; Matějková, J.; Dai, Y. S.; Urbánek, T.; Šlouf, M.; Škorič, M.; Nejedlý, T.; Hrubý, M.; Fang, J. Y., Nanocrystalline chloroxine possesses broad-spectrum antimicrobial activities and excellent skin tolerability in mice. *Nanomedicine (Lond)* **2022,** *17* (3), 137-149.

81. Urbánek, T.; Ivanko, I.; Svoboda, J.; Tomšík, E.; Hrubý, M., Selective potentiometric detection of reactive oxygen species (ROS) in biologically relevant concentrations by a modified metalized polyporphyrine sensing layer coated with nonbiofouling poly(2-alkyl-2oxazoline)s. *Sensors and Actuators B: Chemical* **2022,** *363*, 131827.

6. Appendixes – attached publication

Publication declaration

In all publications included in this thesis, I, Tomáš Urbánek, was responsible for the synthetic procedures and the physico-chemical characterization of the prepared materials. This included techniques such as SEC, UV-Vis spectrophotometry, DLS, and NMR, with advanced NMR measurements conducted with the assistance of Rafał Konefał. The SEM and TEM analyses were performed by Miroslav Šlouf. A4F was carried out by Dmytro Rak and Marián Sedlák at the Institute of Experimental Physics in Košice. Cyclic voltammetry and EIS were conducted by Iryna Ivanko, while Jan Svoboda performed XPS. The biological characterization of the samples was undertaken by collaborating biologists, including Jiří Trousil, Kristýna Gunár, Olga Šebestová Janoušková, Jana Matějková, You-Shan Dai, Jia-You Fang, and Miša Škorič, at various institutions such as the Institute of Macromolecular Chemistry AS CR, the Department of Medical Microbiology at the Second Faculty of Medicine, Charles University, the Pharmaceutics Laboratory at the Graduate Institute of Natural Products, Chang Gung University, and the Department of Pathological Morphology and Parasitology at the Faculty of Veterinary Medicine, University of Veterinary Sciences Brno.